Acta Biomaterialia xxx (xxxx) xxx

Contents lists available at ScienceDirect

Acta Biomaterialia

journal homepage: www.elsevier.com/locate/actbio

Full length article

Antibiotic delivery from bone-targeted mesoporous silica nanoparticles for the treatment of osteomyelitis caused by methicillin-resistant *Staphylococcus aureus*

J.J. Aguilera-Correa[a,b,1], M. Gisbert-Garzarán[a,e,1], A. Mediero[c], M.J. Fernández-Aceñero[d], D. de-Pablo-Velasco[d], D. Lozano[a,e], J. Esteban[b,f,*], M. Vallet-Regí[a,e,*]

[a] *Departamento de Química en Ciencias Farmacéuticas, Universidad Complutense de Madrid, Instituto de Investigación Sanitaria Hospital 12 de Octubre i+12, Plaza Ramón y Cajal s/n, 28040 Madrid, Spain*
[b] *CIBER de Enfermedades Infecciosas (CIBERINFEC), 28029 Madrid, Spain*
[c] *Bone and Joint Unit, IIS- Fundación Jimenez Diaz, UAM, Avenida Reyes Católicos, 2 28037 Madrid, Spain*
[d] *Pathology Department, San Carlos Clinical Hospital, UCM, Madrid, Spain*
[e] *CIBER de Bioingeniería, Biomateriales y Nanomedicina (CIBER-BBN), 28029 Madrid, Spain*
[f] *Clinical Microbiology Department, IIS-Fundación Jiménez Diaz, UAM, Avenida Reyes Católicos, 2 28037 Madrid, Spain*

ARTICLE INFO

Article history:
Received 13 May 2022
Revised 13 October 2022
Accepted 19 October 2022
Available online xxx

Keywords:
Osteomyelitis
Biofilm
Methicillin-resistant *Staphylococcus aureus*
Mesoporous silica nanoparticles
Bone-targeting
Drug delivery

ABSTRACT

Osteomyelitis is a hard-to-treat infection of the bone and bone marrow that is mainly caused by *Staphylococcus aureus*, with an increasing incidence of methicillin-resistant *S. aureus* (MRSA). Owing to the aggressiveness of these bacteria in colonizing and destroying the bone, systemic antibiotic treatments fail to eradicate the infection. Instead, it normally entails surgery to remove the dead or infected bone. In this work, we report bone-targeted mesoporous silica nanoparticles for the treatment of osteomyelitis. The nanoparticles have been engineered with a functional gelatine/colistin coating able to hamper premature release from the mesopores while effectively disaggregating the bacterial biofilm. Because antibiotic resistance is a global emergency, we have designed two sets of identical nanoparticles, carrying each of them a clinically relevant antibiotic, that have demonstrated to have synergistic effect. The bone-targeted nanoparticles have been thoroughly evaluated *in vitro* and *in vivo*, obtaining a notable reduction of the amount of bacteria in the bone in just 24 h after only one dose, and paving the way for localized, nanoparticle-mediated treatment of MRSA-caused osteomyelitis.

Statement of significance

In this work, we propose the use of bone-targeted mesoporous silica nanoparticles to address *S. aureus*-caused osteomyelitis that render synergistic therapeutic effect *via* multidrug delivery. Because the bacterial biofilm is responsible for an aggressive surgical approach and prolonged antibiotic treatment, the nanoparticles have been functionalized with a functional coating able to both disaggregate the biofilm, hamper premature antibiotic release and protect the intact bone. These engineered nanoparticles are able to effectively target bone tissue both *in vitro* and *in vivo*, showing high biocompatibility and elevated antibacterial effect.

1. Introduction

Osteomyelitis is the inflammation of the bone and bone marrow provoked by at least one microorganism, which leads to local bone destruction, necrosis, and apposition of new bone and can compromise bone or joint infection [1]. Though its incidence is approximately 22 cases per 100,000 person-years [2], the implications of this disease are beyond these numbers, including mortality.

* Corresponding authors at: Departamento de Química en Ciencias Farmacéuticas, Universidad Complutense de Madrid, Instituto de Investigación Sanitaria Hospital 12 de Octubre i+12, Plaza Ramón y Cajal s/n, 28040 Madrid, Spain.
E-mail addresses: jesteban@fjd.es (J. Esteban), vallet@ucm.es (M. Vallet-Regí).
[1] Both authors have contributed equally.

https://doi.org/10.1016/j.actbio.2022.10.039
1742-7061/

Although any microorganism can virtually cause osteomyelitis, this infection is mainly caused by Gram-positive bacteria, such as *Staphylococcus aureus*, which is responsible for up to 90% osteomyelitis cases [1]. Of them, up to 28% are methicillin-resistant *Staphylococcus aureus* (MRSA) [3], which makes MRSA a common causative pathogen in this type of infection [4]. Given the MRSA antibiotic resistance, "MRSA infections continue to be a major public health concern", according to a recent World Health Organization (WHO) report (*Global antimicrobial resistance and use surveillance system report: 2021*) [5]. MRSA usually shows high resistance to co-trimoxazole, ciprofloxacin and erythromycin [6].

S. aureus can invade the osteocyte lacuno-canalicular network of the cortical bone and persist in the bone [7,8]. This invasion is possible thanks to durotaxis and haptotaxis, which are motility events guided by bone stiffness [9], or caused by a gradient of staphylococcal adhesion [10], respectively. This pathogenic mechanism is responsible for the high recurrence of this infection [11], that can re-emerge up to 75 years after first *S. aureus* infection [12]. Besides, this infection involves biofilm development, a bacterial state that favours bacterial survival against adverse situations, such as phagocytosis by phagocytic immune cells, or antibiotics, among others [7]. Because of this form of bacterial growth, osteomyelitis treatments usually include both surgical removal of infected or dead bone and intravenous antibiotic administration. For all this, osteomyelitis is considered a hard-to-treat infection [13].

In the last years, the field of nanomedicine has grabbed the attention of many scientists and it is expected to revolutionize the pharmaceutical and biotechnological industries soon. In this sense, up to 75% of approved nanomedicines are nanoparticles acting as drug delivery carriers [14]. The main rationale for using nanoparticles is that therapeutics can be loaded within them, ideally releasing the cargo only at the diseased area. Hence, nanoparticles hold the potential to minimize the side effects on healthy cells associated to the free drugs and would abrogate the need to use high free drug doses to achieve therapeutic efficacy. Among the different types of nanoparticles, mesoporous silica nanoparticles (MSNs) present relevant features that make them promising candidates for drug delivery. In this regard, MSNs have been applied to the development of new treatments against complex bone diseases, such as osteoporosis, bone cancer and bone infection [15]. Aside from biocompatibility, MSNs present physicochemical properties that are interesting for antibiotic delivery. The large surface areas (*ca.* 1000 m^2/g) and pore volumes (*ca.* 1 cm^3/g) allow the adsorption of high amounts of drug molecules. In addition, being able to tune the pore size and morphology allow to design MSNs that could specifically load low (*e.g.*, moxifloxacin) or high (*e.g.*, vancomycin) molecular weight antibiotics [16–19].

Despite those features, MSNs have been scarcely explored as carriers for treating osteomyelitis. Huang et al. produced a composite containing levofloxacin-loaded MSNs that inhibited bacterial adhesion and growth both *in vitro* [20] and *in vivo* [21], although requiring surgical intervention for the administration. Nie et al. [22] used bone-targeted, vancomycin-loaded MSNs using both D_6 and UBI29-41 peptides, to treat a murine model of osteomyelitis. Despite the good outcome, the *S. aureus* infection on the implant was let to grow just for 24 h, what makes the infection more susceptible to the intravenously administrated therapy and does not reflect a realistic scenario where the infection is causing an abscess. Hence, such approach would not represent accurately the actual features of osteomyelitis. Instead, the biofilm-infected implants employed in this manuscript induce the formation of intraosseous abscess, which is a histological finding commonly associated with osteomyelitis [23]. In consequence, the novelty of our work not only relies on the accuracy of the osteomyelitis model employed and the lack of surgical intervention, but also on the cooperative multidrug delivery from the bone-targeted nanoparticles, which present themselves antibiofilm features that would facility the treatment of the resistant bacteria on infected bone.

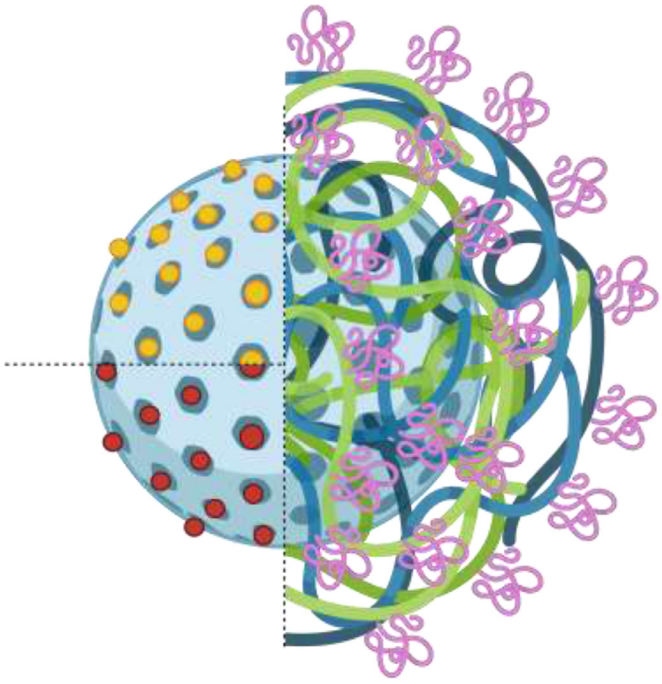

Scheme 1. Schematic representation of the mesoporous silica nanoparticles (grey) loaded with moxifloxacin (yellow) or rifampicin (red), coated with gelatine (blue) plus colistin (green) and decorated with aspartic acid hexapeptides (pink). (For interpretation of the references to colour in this figure legend, the reader is referred to the web version of this article.)

In this work, we have addressed the treatment of *S. aureus*-caused osteomyelitis using MSNs engineered for achieving bone-targeted synergistic multidrug delivery (Scheme 1). To avoid any undesirable chemical interactions between the antibiotics, we have designed two sets of identical nanoparticles differing in the antibiotic loaded within the pores (moxifloxacin (MX) or rifampicin (RI). Even though RI is a remarkable antistaphylococcal agent in biofilm-related infections, it cannot be clinically employed as monotherapy. In this regard, we have demonstrated that the multidrug approach improved the individual performances. In addition, since premature antibiotic release would result in the treatment being ineffective, the MSNs have been coated with a biocompatible coating containing enzymatically degradable gelatine and colistin (CO), an antibiotic with biofilm-disaggregating features. Minimizing premature drug release is of major importance, since otherwise there would be no clinical difference between the free drug and the drug uncontrollably released from the nanoparticles, which might not reach the diseased area. Furthermore, because the nanoparticles might be rapidly cleared from the bone, they have been further decorated with an aspartic acid hexapeptide (D_6) to provide affinity toward bone tissue and guarantee that the treatment remains in the diseased area long enough for the drugs to be released [22]. Finally, the bactericidal effect of this biocompatible nanocarrier has been extensively analysed *in vitro* and *in vivo*, including various models of bone infection, showing promising results with just one dose, and paving the way for improved treatments of MRSA-caused osteomyelitis. To the best of our knowledge, this is the first example ever reported of a bone-targeted nanocarrier capable of exerting synergistic antibacterial affect along with remarkable antibiofilm features with demonstrated efficacy against MRSA-caused osteomyelitis.

2. Materials and methods

2.1. Synthesis of MCM-41 mesoporous silica nanoparticles

The following compounds were purchased from Sigma-Aldrich (USA): Tetraethyl orthosilicate (TEOS); Ammonium nitrate; Cetyltrimethylammonium bromide (CTAB); Fluorescein isothiocyanate (FITC); Rhodamine B isothiocyanate (RhB); 3-(Aminopropyl)triethoxysilane (APTES).

Mesoporous silica nanoparticles were produced using a modification of the Stöber method [24]. Briefly, CTAB (2.74 mmol, 1 g) was placed in a 1-L flask and NaOH (2M, 3.5 mL) and H_2O (480 mL) were added and heated to 80 °C. Afterward, TEOS (22.39 mmol, 5 mL) was dropwisely added (0.33 mL/min) and the mixture was stirred at 80 °C for further 2 h. Then, the nanoparticles were centrifuged and washed twice with water and once with ethanol. The CTAB template was eliminated by ionic exchange, employing a solution of NH_4NO_3 (10 mg/mL) in ethanol (95%). For that purpose, the MSNs were dispersed in 350 mL of that solution, refluxed for 3 h and subsequently collected by centrifugation and washed with water and ethanol. The whole process was repeated two times. Finally, the surfactant-free nanoparticles were kept in absolute ethanol until the different functionalization steps were carried out.

The biological experiments were performed using either FITC- or RhB -labelled MSNs. For this purpose, FITC (0.002 mmol, 0.78 mg) or RhB (0.002 mmol, 1.07 mg) were reacted with APTES (0.009 mmol, 2.2 µL) in 40 µL of ethanol for 2 h. Then, the mixture was mixed with TEOS (22.39 mmol, 5 mL) and the MSNs were synthesized following the above-described methodology.

The nanoparticles were characterized by means of Thermogravimetric Analysis (TGA), Fourier Transformed Infrared (FTIR) spectroscopy, Zeta potential and Dynamic Light Scattering (DLS). TGA measurements were carried out in a Perkin Elmer Pyris Diamond TG/DTA analyser, applying 5 °C/min heating ramps from rt to 600 °C. FTIR spectra were collected in a Nicolet Nexus (Thermo Fisher Scientific) equipped with a Goldengate attenuated total reflectance device, averaging 64 scans in the range 4000-400 cm^{-1} (resolution 1 cm^{-1}). Zeta potential and DLS measurements were performed in a Zetasizer Nano ZS (Malvern Instruments) equipped with a 633 nm laser. Samples were dispersed in distilled water and placed in a DTS1070 disposable folded capillary cell (Malvern instruments) for data acquisition.

2.2. Gelatine coating of nanoparticles

The gelatine (GE) coating was performed by modifying a methodology previously described [25]. The use of GE is based on the staphylococcal ability to degrade it and use it as carbon source [26,27]. MSNs were initially functionalized with GE in the absence of antibiotics to optimize the coating conditions. Briefly, a GE solution (0.5 %, w/v) was prepared by dissolving 100 mg of type B GE powder from bovine skin (Sigma Aldrich, USA) in 20 mL phosphate buffer saline (PBS) (pH=7.4) (Lonza, Switzerland). The solution was stirred at 45 °C for 30 min. Then, 1 mL of that solution was placed in a 4-mL vial under vigorous stirring at room temperature, to which a dispersion of MSNs was rapidly added (1 mL, 12 mg/mL of MSNs in PBS). The whole mixture was stirred for 5 min. Finally, the nanoparticles were centrifuged and washed twice with PBS at 0 °C, leading to GE-coated MSNs.

For the synthesis of GE+CO-coated MSNs, 50 mg of colistin sodium methanesulfonate (Sigma Aldrich, USA) were mixed with the GE solution prior to the addition of the nanoparticles. Then, the coating was carried out as described above to yield GE+CO-coated MSNs. CO is a polymyxin agent (polymyxin E) that is only effective against Gram-negative infections [28]. Regardless, CO can destabilise the *S. aureus* biofilm matrix structure and lead to the release of planktonic cells, making them more susceptible to antibiotics [29].

The functionalized nanoparticles were characterized in terms of Fourier Transformed Infrared (FTIR) spectroscopy, Thermogravimetric Analysis (TGA), Transmission Electron Microscopy (TEM), Dynamic Light Scattering (DLS) and Zeta potential. TEM images were taken on a JEOL JEM 1400. Samples were dispersed in distilled water under sonication and then a few drops were deposited onto carbon-coated copper grids.

2.3. Antibiotic loading into the nanoparticles and antibiotic release

2.3.1. Antibiotic loading

The different nanoparticles were loaded by shaking them in the presence of a saturated solution of the corresponding antibiotic. To produce MX-loaded nanoparticles, 12 mg of MSNs were dispersed in 1 mL of a 10 mg/mL solution of moxifloxacin (Sigma Aldrich, USA) (MX) in distilled water for injection (B. Braun, Germany). To produce RI-loaded nanoparticles, 12 mg of MSNs were dispersed in 1 mL of a 10 mg/mL solution of rifampicin (Sigma Aldrich, USA) (RI) in chloroform (Sigma Aldrich, USA). Then, each solution was stirred at 1,400 rpm and 5 °C for 24 h [30]. Afterward, antibiotic-loaded MSNs were centrifuged, and the supernatant was removed. The MX-loaded MSNs were dried at 60 °C for 3 h, whilst RI-loaded MSNs were dried at room temperature for 2 h. After loading each antibiotic, the MSNs were coated with GE+CO as described above.

The rationale for using MX is that it is a broad spectrum, fourth-generation fluoroquinolone antibacterial antibiotic, effective against both Gram-negative and Gram-positive bacteria [31], that is commonly used in monotherapy to treat bone-related infections [32–34]. Similarly, the use of RI relies on the fact that it is a broad spectrum polyketide belonging to ansamycins that is effective against both Gram-negative and Gram-positive bacteria. However, it needs to be used in combination with another antibiotic [35]. In addition, it is a potent antistaphylococcal [36–38].

2.3.2. Antibiotic release

To determine the drug release from the nanoparticles, 12 mg of the corresponding antibiotic-loaded MSNs were suspended in 1 mL of PBS. Then, each suspension was placed with another mL of PBS into the lower chamber of a 6-well plate Transwell® (Corning, USA). Then, the upper chamber was placed, and 1 mL of PBS was added. This buffer was selected because it is one of the most used solutions for evaluating antibiotic release from nanomaterials [39–43]. The final concentration of nanoparticles was 4 mg/mL per well (n = 4). The plate was incubated at 37 °C and 5% CO_2. Periodically, 300 µL from each upper chamber were removed for analysis and replaced by 300 µL of fresh PBS. MX concentration was determined by measuring the fluorescence using an excitation wavelength of 294 nm and an emission wavelength of 503 nm [44], whereas that of RI was quantified by measuring the absorbance at a wavelength of 475 nm [45]. To estimate the percentage of antibiotic released from each nanoparticle, the values were normalized to the total amount of antibiotic collected at the end of the experiment (24 h). This experiment was conceived to demonstrate that the GE coating could slow down the antibiotic release in the absence of stimulus, compared to the same uncoated nanoparticles. The kinetics were studied for 24 h to match the time that the animals would be receiving the treatment.

CO was labelled with FITC (CO-FITC) to monitor the release. CO was selected because it is a polymyxin agent that has been shown to destabilize the *S. aureus* biofilm, leading to the release of planktonic cells that are more susceptible to antibiotics [29]. For that purpose, 50 mg of colistin and 0.1 mg of FITC were dissolved in DMSO and stirred overnight at room temperature. The

mixture was then precipitated in cold ether/acetone (90:10), centrifuged and washed with ethanol until no FITC was observed in the supernatant.

To determine CO release, 12 mg of GE+CO-coated MSNs were placed in the presence or absence of *S. aureus*. A control group containing MSNs just coated with CO was also employed. CO-FITC MSNs were suspended in 1 mL of PBS to evaluate the release kinetics. This millilitre was placed with another millilitre of PBS with or without a 0.5 McFarland suspension in PBS of SAP231 into the lower chamber of a Transwell® 6-well plate. Then, the upper chamber of the Transwell® 6-well plate was placed and 1 mL of PBS was added. The final concentration of nanoparticles was 4 mg/mL per well (n=3). The plate was incubated at 37 °C and 5% CO_2. Regularly, 300 µL of each upper chamber were sampled and replaced by 300 µL of new PBS. These 300 µL were used to determine colistin-FITC concentration by measuring the fluorescence using an excitation wavelength of 490 nm and an emission wavelength of 525 nm.

2.4. Peptide grafting

First, the GE coating of GE+CO-coated MSNs was partially thiolated (GE+CO-coated MSNs-SH). For that purpose, 12 mg of GE+CO-coated MSNs were dispersed in 1 mL of cold PBS containing 16 mg/mL of 2-Iminothiolane hydrochloride (Sigma Aldrich, United States). The mixture was incubated with stirring and at room temperature for 1 h. After that, the nanoparticles were centrifuged, washed with 1 mL of cold PBS, and dispersed again in 1 mL of cold PBS containing 4 mg/mL of aspartic acid hexapeptide (D_6) N-terminal modified with a 6-maleimidohexanoic acid (Abyntek Biopharma S. L., Spain). The D_6 peptide shows affinity for hydroxyapatite, an inorganic component of hard tissues, such as bone or teeth [46]. The mixture was incubated at 750 rpm and room temperature for 1 h. Finally, the nanoparticles were centrifuged and washed with 1 mL of cold PBS at 4 °C, leading to D_6-decorated GE+CO-coated MSNs (D_6-GE+CO MSNs).

2.5. Affinity of D_6 toward bone

To highlight the affinity of D_6 toward bone, 1 mL of PBS containing 2 mg/mL of either GE-coated or D_6-GE+CO-coated MSNs was incubated with 25 mg of bovine trabecular bone (Bio-Oss Spongiosa from 0.25 to 1mm; Inibsa, Spain) at 750 rpm and at 37 °C for 2 h. After this, the bone was washed three times with 1 mL of PBS. The bone was directly analysed in a Leica SP-2 AOBS confocal laser-scanning microscope (Leica, Germany). The nanoparticles were labelled with rhodamine B (Sigma Aldrich) to allow visualization under the microscope.

2.6. Microbiological studies

A methicillin-resistant *S. aureus* strain (SAP231) was used in all microbiological studies. This strain can produce bioluminescence *per se* [47]. The strain was kept frozen at –80 °C until the experiments were performed. The purity of its axenic culture was corroborated every day by inoculating each broth on a blood tryptic-soy agar (Biomérieux, France). The purity of each experiment was assessed by seeding each replicate of each condition in TSA supplemented with blood and checking that the *S. aureus* strain morphology was the same. In case of doubt, the strain was identified by using Matrix-Assisted Laser Desorption/Ionization -Time-Of-Flight (MALDI-TOF, Vitek® MS, Biomérieux, France).

2.7. Bacteria-nanoparticles interaction

The SAP231-nanoparticle interaction was evaluated through four different experiments: (1) evaluation of whether the GE coating can be employed as carbon source by SAP231, (2) evaluation of the influence of the nanoparticle coating on the SAP231 biofilm development, (3) analysis of the interaction between the grown SAP231 biofilm and the nanoparticles, and (4) evaluation of whether SAP231 can trigger drug release from GE-coated nanoparticles.

To evaluate the use of the coating as carbon source by SAP231, 75 µL of PBS containing 20 mg/mL of either MSNs or GE-coated MSNs were deposited in a well of a luminescence Hard-Shell® 96-Well PCR Plate (Bio-Rad, United States). Then, 75 µL of 1.07 McFarland suspension in PBS were added. PBS supplemented with 1% (p/v) of GE was used as positive control. Then, the plate was statically incubated at 37 °C and 5% CO_2 for 1 h. After incubation, bioluminescence was measured in a EnSpire multimode plate reader (Pelkin Elmer, United States). This experiment was performed by duplicate and four times (n=8 per condition).

To evaluate the effect of the nanoparticle coating on the biofilm development of SAP231, 100 µL of 1.07 McFarland suspension in 0.9% NaCl saline (B. Braun, Germany) were adhered on the bottom of a 96-well flat-bottom plate at 37 °C and 5% CO_2 for 90 min. Thereafter, the supernatant was removed, and each well was washed with 200 µL of sterile saline twice. Finally, 150 µL of TSB supplemented with 1% glucose with or without uncoated, GE-coated or GE+CO-coated MSNs were added (n=8 per condition). This medium is a widely recognized inducer of biofilm formation in bacteria [48]. The plate was incubated at 37 °C and 5% CO_2 for 24 h, which is the incubation time generally employed in the field to obtain a *S. aureus* mature biofilm. After that, each well was rinsed with 200 µL of saline and stained with 2% of crystal violet, according to a previously reported methodology [48]. The experiment was performed in triplicate (n=24 per condition).

To evaluate the effect of the nanoparticle on a SAP231 mature biofilm, 100 µL of 1.08 McFarland suspension in 0.9% NaCl saline (B. Braun, Germany) were adhered on the bottom of a 96-well flat-bottom plate at 37 °C and 5% CO_2 for 90 min to generate a biofilm. Thereafter, the supernatant was removed, each well was washed with 200 µL of sterile saline twice and 200 µL of TSB supplemented with 1% glucose were added. The plate was incubated at 37 °C and 5% CO_2 for 24 h. The supernatant was then removed, and each well was rinsed twice with 200 µL of saline. Then, 200 µL of saline with or without uncoated and GE- or GE+CO-coated MSNs were added to each well, and the plate was incubated at 100 rpm at 37 °C for 30 min. After that, each well was rinsed again with 200 µL of saline and stained with 2% of crystal violet. The experiment was performed in triplicate (n=24 per condition).

To gain insight into the effect of GE on the SAP231 biofilm development, the expression of different proteases (aureolysin, staphopain, ssp 8V protease and splF) and a transcription factor (rot factor) during biofilm development was evaluated. The biofilm formation was induced in 2 mL of TSB + 1% glucose in presence or absence of 10% of bovine GE at 37 °C for 24 h, as described above. The 2 mL were centrifuged after incubation, and the mRNA was extracted using TRIzol™ Max™ Bacterial RNA Isolation Kit (Thermo Fisher Scientific, United State). A real time PCR was done using SYBER Green Master Mix (Qiagen, United States), employing the primers described by Mootz et al. to detect specific transcripts [49]. Gene expression was normalized by the endogenous control (16S rRNA). Results were expressed in mRNA copy numbers, calculated for each sample using the cycle threshold (Ct) value, and normalized by bacteria grown in TSB+1% glucose without bovine GE. The relative gene expression was represented by $2-\Delta\Delta Ct$, where $\Delta\Delta Ct = \Delta Ct$ target gene $-\Delta Ct$ 16S RNA. The fold change for the bacteria grown in presence of bovine GE was defined as the relative expression compared with bacteria grown in absence of bovine gelatine. The latter was calculated as $2-\Delta\Delta Ct$, where $\Delta\Delta Ct = \Delta C$ bacteria grown in presence of bovine gelatine

$-\Delta C$ bacteria grown in absence of bovine GE. This experiment was performed five times. Of note, it was not possible to perform this experiment using any type of MSNs at the concentration chosen (10 mg/mL) because they interfered with RNA extraction.

To evaluate whether SAP231 could trigger the drug release from GE-coated MSNs, 12 mg of MSNs were loaded with 500 µL of propidium iodide (PI) in water (500 µg/mL) (Sigma Aldrich, USA) at 1,400 rpm at 5 °C for 24 h. Then, the nanoparticles were centrifuged and rinsed once with 1 mL of distilled water. After this, 12 mg of each PI-loaded MSNs were suspended in 1 mL of brain-heart infusion (BHI) (BD, USA) to determine the PI release from either uncoated or GE-coated MSNs. This suspension was mixed with 1 mL 1.08 McFarland suspension of SAP231 into the lower chamber of a Transwell® 6-well plate. Then, the upper chamber of the Transwell® 6-well plate was inserted and 1 mL of BHI was added. The final concentration of nanoparticles was 6 mg/mL per well. The plate was incubated at 37 °C and 5% CO_2. Periodically, 300 µL of each upper chamber were sampled and replaced by 300 µL of sterile BHI. These 300 µL were used to determine the PI concentration by measuring the fluorescence using an excitation wavelength of 493 nm and an emission wavelength of 636 nm. A calibration curve ranging from 250 to 0.122 µg/mL was employed. The bacterial concentration was estimated by using a well of a 6-well plate with the same bacterial concentration but without MSNs and measuring the SAP231 luminescence. This experiment was performed in triplicate.

2.8. Minimal inhibitory concentration and minimal bactericidal concentration

Minimum inhibitory concentrations (MIC) were determined using the previously described broth microdilution method [50] with one modification. The MIC is the minimum concentration required to inhibit the bacterial visible growth. In brief, a series of nanoparticle concentrations ranging from 1,000 µg/mL to 0.9765 µg/mL with a two-fold dilution were added to cation adjusted Müller-Hinton broth (Sigma Aldrich, USA) (CAMHB) to a final volume of 100 µL per well. One hundred µL of bacterial suspension in CAMHB containing approximately 1.6×10^6 colony-forming units per mL (CFU/mL) were added to a Costar 96-well round-bottom polypropylene plate (Corning Inc., USA) followed by static incubation at 37 °C and 5% CO_2 for at least 20 h. After incubation, MIC was determined by the naked eye as the well with the lowest concentration of nanoparticles where no bacterial growth was observed. Minimum bactericidal concentration (MBC) was determined using the flash microbiocide method [51]. The MBC is defined as the minimum concentration required to kill a certain bacterial concentration. Briefly, 20 µL of each well from the MIC 96-wells plate were mixed after 24-h incubation with 180 µL of tryptic soy broth (TSB) in a new 96-well plate, which was incubated statically at 37 °C and 5% CO_2 for 24 h. After incubation, MBC was determined by the naked eye as the well with the lowest concentration of MSNs where no bacterial growth was observed. The experiments were performed four times.

2.9. Minimal biofilm inhibitory concentration and minimal biofilm eradication concentration

Minimal biofilm inhibitory concentrations (MBIC) and minimal biofilm eradication concentrations were determined using a methodology previously described [52]. The MBIC is the minimum concentration required to inhibit the visible growth of a bacterial biofilm. For MBIC, biofilm was formed by inoculating 100 µL of CAMHB containing 10^6 CFU/mL of bacteria on the bottom of the wells of a 96-well flat-bottom plate (Thermo Fisher Scientific, United States). The plate was statically incubated at 37 °C and 5% CO_2 for 24 h. After incubation, the supernatant was removed. Afterwards, each well was filled with 200 µL of CAMHB containing different concentrations of the corresponding nanoparticles, ranging from 1,000 µg/mL to 0.9765 µg/mL with a two-fold dilution. The plate was statically incubated at 37 °C and 5% CO_2 for at least 20 h. After incubation, MBIC was determined by adding 20 µL of 5 mg/mL of MTT (3-(4,5-dimethylthiazol-2-yl)-2,5-diphenyltetrazolium bromide) tetrazolium assay and incubating at 37 °C for 30 min [53]. After incubation, 100 µL of the supernatant from each well were carefully aspirated and deposited in a new 96-well plate. MBIC was determined by the naked eye as the well with the lowest concentration of nanoparticles where no colour change could be observed. The MBEC is the minimum concentration required to kill a bacterial biofilm. For MBEC, the bottom of each well was scrapped with a 100-µL tip to detach physically the biofilm from the bottom surface of each well and 20 µL of each well were transferred to a new well containing 180 µL of TSB. The plate was incubated statically at 37 °C and 5% CO_2 for 24 h. After incubation, MBEC was determined by the naked eye as the well with the lowest concentration of nanoparticles where no bacterial growth was observed. The experiments were performed four times.

2.10. Interaction between the antibiotics loaded in the nanosystems

The combined therapeutic effect of D_6-GE+CO-coated MX-loaded MSNs and D_6-GE+CO-coated RI-loaded MSNs on SAP231 biofilm was assessed by using the checkerboard [54,55]. This methodology is supported by the European Committee on Antimicrobial Susceptibility Testing (EUCAST) [56]. The interaction between both antibiotics may be quantified by the fractional inhibitory concentration (FIC) [57].

2.11. In vitro *anti-biofilm efficacy of GE+CO-coated antibiotic-loaded MSNs in a model of bone infection*

The anti-biofilm efficacy of each loaded GE+CO-coated MSNs was evaluated using a model of bone infection made from wound-like medium [58]. Briefly, the wound-like medium is composed of 45% Bolton broth (Sigma Aldrich, United States), 50% bovine serum adult (Sigma Aldrich, United States), and 5% laked horse red blood (ThermoFisher Scientific, United States) [59]. First, a 2-mL tube with 10 mg of bovine trabecular bone was rinsed with 1 mL of saline. Then, 500 µL of saline with 3.15×10^8 CFU/mL were added to each tube and were incubated statically at 37 °C and 5% CO_2 for 1.5 h. The supernatant was then removed, and each tube was rinsed twice with 1 mL of saline. Afterward, 1 mL of wound-like medium was placed into each tube, which were further incubated statically at 37 °C and 5% CO_2 for 48 h. The use of bovine trabecular bone and wound-like medium mimics *in vitro* the conditions where a staphylococcus causing osteomyelitis would grow *in vivo*. After biofilm formation, each tube was rinsed twice with 1 mL saline and treated in presence or absence of two different concentrations of nanoparticles dispersed in 1 mL of saline, which were further incubated statically at 37 °C and 5% CO_2 for 24 h. The concentration of D_6-GE+CO-coated MX-loaded MSNs (125 µg/mL) was estimated according to the MIC obtained, and considering previous studies that stablish 4×MIC as a good therapeutic approach [58,60,61]. Given the low values of MIC obtained for D_6-GE+CO-coated RI-loaded MSNs, it was decided to evaluate three concentrations: the same concentration of D_6-GE+CO-coated MX-loaded MSNs (125 µg/mL), and two two-fold dilutions (62.5 and 31.25 µg/mL). After incubation, each tube was rinsed twice with 1 mL of saline and all trabecular bone from each tube was transferred to a 5 mL round-bottom tube containing 1 mL of saline. All tubes were sonicated at room temperature for 5 min [62]. Then, the number of bacteria was determined as CFU per gram of bone by using

the drop plate method [63] in Chapman agar plates (BioMérieux, France). The plates were incubated at 37 °C and 5% CO_2 for at least 24 h. The experiment was performed five times.

To support visually the numerical results, the previous experiment was also analysed using scanning electron microscopy (SEM). For SEM observation, the same samples were fixed with 2.5% glutaraldehyde in 0.1 M sodium cacodylate buffer at pH 7 at 4º C for 90 min. Samples were then dehydrated with increasing concentrations of ethanol (30, 50, 70, 90, and 100%) at 22 °C for 10 min. Micrographs were obtained using a field emission gun JEOL JSM6400 scanning electron microscope (Jeol Ltd, Tokyo, Japan).

2.12. In vitro *prevention of bone infection*

To demonstrate the preventive ability of the D6-GE+CO-coated antibiotic-loaded MSNs adhered on the bone, 10 mg bovine trabecular bone were incubated with 350 µL of 2 mg/mL of D6-GE+CO-coated MX-loaded and RI-loaded MSNs in PBS were incubated at 750 rpm and at 37 °C for 2 h. After this, the bone was washed three times with 500 µL of PBS. Thereafter, 500 µL of wound-like medium with a 1:100 dilution of a 0.48 McFarland suspension of SAP231 in saline were added. The whole system was statically incubated at 37 °C and 5% CO_2 for 24 h. Non-treated bovine trabecular bone was used as positive control. After incubation, each tube was rinsed twice with 1 mL of saline and all trabecular bone from each tube was transferred to a 5 mL round-bottom tube containing 1 mL of saline. All tubes were sonicated at room temperature for 5 min [62]. Then, the number of bacteria was determined as CFU per gram of bone by using the drop plate method [63] in Chapman agar plates (BioMérieux, France). The plates were incubated at 37 °C and 5% CO_2 for at least 24 h. The experiment was performed five times. This experiment was also visualized using SEM according to the above-mentioned methodology.

2.13. Cell studies

For the cell studies, MC3T3-E1 and RAW264.7 cells obtained from American Type Culture Collection (ATCC) were used. The cells were stored in liquid nitrogen until the experiments were carried out. MC3T3-E1 were inoculated at a concentration of 10,000 cells/cm^2 on 96-well plates with α-minimum essential medium containing 10% foetal bovine serum and 1% penicillin-streptomycin (αMEM, Invitrogen, Thermo Fisher Scientific). RAW264.7 cells were seeded at a concentration of 5,000 cells/cm^2 on 96-well plates with α-minimum essential medium containing 10 % foetal bovine serum and 1% penicillin-streptomycin (αMEM, Invitrogen, Thermo Fisher Scientific Inc. USA). After cell adherence, MC3T3-E1 cells medium was replaced by αMEM containing 50 mg/mL ascorbic acid (Sigma-Aldrich, USA) and 10 mM ß-glycerol-2-phosphate (Sigma-Aldrich, USA). Part of the RAW264.7 cells was incubated in the presence of 50 ng/mL of Receptor Activator for Nuclear Factor κ B Ligand (RANKL) (R&D Systems, Bio-Techne, Madrid, Spain) to promote osteoclast differentiation. During incubation, all the cells were kept in the incubator at 37 °C, 5% CO_2, and 95% humidity. All types of cells (MC3T3-E1, RAW264.7 and RAW264.7 osteoclast precursors) were treated with 125 µg/mL of D_6-GE+CO-coated MX-loaded MSNs and 62.5 µg/mL of D_6-GE+CO-coated RI-loaded MSNs (n=24 per concentration). These nanoparticle concentrations were chosen based on the microbiological susceptibility results. Non-treated cells incubated with just growth medium were considered as control (n=24). The cytotoxicity was tested by CytoTox 96® Non-Radioactive Cytotoxicity Assay (Promega, USA) after 48 h of incubation, according to previously published methodology [64]. To evaluate the cytotoxic effect of the nanosystem over time, cells exposed for 48 h to the nanosystem were incubated for further 24 h (72 h in total), or 48 h (96 h). The cell metabolic activity of MC3T3-E1 [65] and RAW cells [66,67] was studied at 2 and 4 days, respectively, through the MTT method. For that purpose, 20 µL of a 5 mg/mL solution of MTT were added to each well and the cells were further incubated for 4 h at 37 °C and 5% CO_2 [68]. Data were represented as relative metabolic activity of each treatment compared to the control, which was considered as 100% of cell metabolic activity.

2.14. In vivo *model*

This study was approved by the Instituto de Investigación Sanitaria of Fundación Jiménez Díaz (IIS-FJD) Animal Care and Use Committee, which includes ad hoc members for ethical issues. Animal care and maintenance complied with institutional guidelines as defined in national and international laws and policies (Spanish Royal Decree 53/2013, authorization reference PROEX109.7/21 July 18, 2021, by the Ministry of the Environment, Local Administration and Territorial Planning of the Community of Madrid and, Directive 2010/63/EU of the European Parliament and of the Council of September 22, 2010).

Specific pathogen-free New Zealand white male rabbits (Granja San Bernardo, Navarra, Spain) of between 2.5 and 3 Kg of weight were used. All animals were housed in individual cages in an air-conditioned room at 22±2 °C and light-darkness cycles of 12:12 h.

The *in vivo* model was based on a study previously published [58] with modifications.

2.15. In vivo *evaluation of nanosystem affinity toward bone*

Two rabbits were subjected to general anaesthesia and treated with a 4-mL intraosseous injection containing 187.5 µg/mL of unloaded D6-GE+CO-coated MSNs suspended in saline by using a 1.5-cm needle and Arrow® EZ-IO® Intraosseous Vascular Access System (Teleplex, Ireland) in the right lateral condyle. One of the animals was euthanized 1 h after the injection and the other one after 24 by intravenous overdose of sodium thiobarbital under general anaesthesia. The spleen, liver, a kidney, and a femur were recovered for each animal. All organs except the femur were fixed, paraffin-infiltrated, and haematoxylin-eosin-stained.

Femurs were fixed for 72 h and were dehydrated with 70, 90, 96 and 100% ethanol for 24 h per concentration. Portions of each femur were included in a transparent two-component embedding resin based on methyl methacrylate (Technovit 4004, Kulzer Technik, Germany), and sanded to a thickness of 200–300 µm by Arte-Lab S. L. (Madrid, Spain). Femur slices were directly analysed in a Leica DM IRB confocal laser-scanning microscope (Leica, Germany) without staining. Nanoparticles were detected thanks to the FITC covalent labelling of the D_6-GE+CO-coated MSNs. Bones were observed using the reflected light.

2.16. Osteomyelitis model

The SAP231 *S. aureus* strain was employed for this *in vivo* model. Each animal was placed in the supine position under general anaesthesia and its hind leg was immobilised and isolated in a sterile field. Skin and muscles were sectioned until the lateral epicondyle was reached. A hole 3.2 mm in diameter and 1 cm deep was drilled. Two 5-mm-long and 0.6-mm-diameter cylindrical Ti-6Al-4V implant infected with a 24-h SAP231 biofilm were placed. To induce that infection, each implant was incubated with 200 µL of a 1:100 dilution of a 1.25 McFarland suspension of SAP231 in a well of a 96-well plate at 37 °C and 5% CO_2 for 24 h. After incubation, each implant was washed with 200 µL of saline (B. Braun, Germany). The number of bacteria per implant was 6.82±0.28 CFU per square centimetre (CFU/cm^2). After lodging the infected implant in the bone marrow, the hole was closed with Ethicon bone

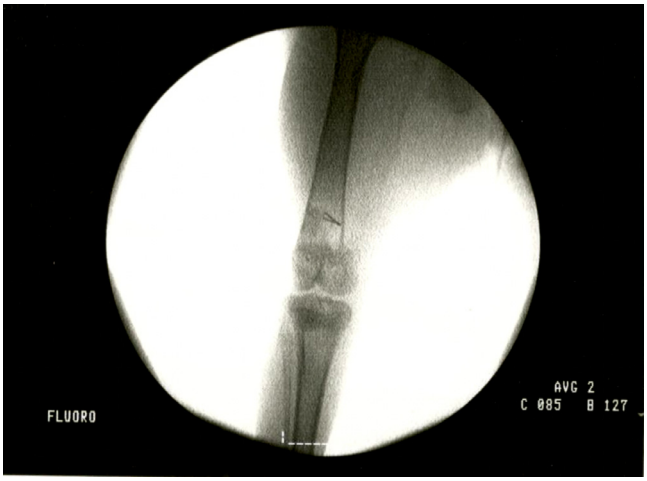

Fig. 1. Anteroposterior fluoroscopy of a rabbit femur with the two infection seeds inside femoral bone marrow.

wax (Johnson & Johnson, United States). The entire area was disinfected with 6-volume hydrogen peroxide. The wound was closed with a continuous cross suture using a 3/0 Prolene suture (Johnson & Johnson, United States). The correct location of the implant was corroborated through dorsoventral (Fig. 1) fluoroscopy of each animal. The behaviour, temperature and weight of each animal were monitored every 24 h throughout the experimental procedure.

The infected animals were randomly assigned to two groups, namely control group (n=7) and D_6-GE+CO-coated antibiotic-loaded MSNs treated group (n=7). The sample size was estimated by Wilcoxon Mann-Whitney test and an a-priori type of power analysis considering d=2.00, α=0.05, (1-β)=0.95, allocation ratio=1 by using G*Power 3.1.9.7 software [69]. The d parameter assumes that D_6-GE+CO-coated antibiotic-loaded MSNs treatment can reduce the MRSA concentration by at least 90% per gram of bone when compared to the control group. The statistical power of the sample was 0.963.

Two days after the surgery, each animal from the treated group was anaesthetized and the infected femur was treated with the antibiotic-loaded nanoparticles. For that purpose, 4 mL of saline containing 500 µg of D6-GE+CO-coated MX-loaded MSNs (*ca.* 6.77 µg/mL of MX) and 250 µg of D6-GE+CO-coated RI-loaded MSNs (*ca.* 2.38 µg/mL of MX) were administered by using a 1.5-cm needle and Arrow® EZ-IO® Intraosseous Vascular Access System. The control group received no treatment. All animals were euthanized after 24 h by intravenous overdose of sodium thiobarbital under general anaesthesia. The femur, liver and a kidney were recovered through sterile preparation. The femurs were decontaminated by addition of 200 mL of with 6-volume hydrogen peroxide for 10 min. Then, they were washed with 250 mL of sterile saline and were deposited in a sterile plastic bag. Each femur with the implant was smashed with a hammer. The medial condyle was used for determining bioluminescence by using an *in vivo* imaging system (IVIS Lumina Series III; PerkinElmer Inc., USA). Finally, those medial condyles were fixed, paraffin-infiltrated, and haematoxylin-eosin stained.

The remaining parts of the femur were smashed, immersed in sterile saline and sonicated using an Ultrasons-H 3000840 low-power bath sonicator (J. P. Selecta, Barcelona, Spain) at 22 °C for 5 min [62]. The resulting sonicate was diluted in a 10-fold dilution bank and seeded on blood-chocolate agar (Biomérieux, France) using the spread plate method [39,70]. The concentration of bacteria was estimated as CFU/g of bone.

The liver and one kidney of each animal were preserved for pathological studies. Histological sections were fixed, paraffin-infiltrated, and haematoxylin-eosin stained.

2.17. Statistical analysis

Statistical analyses were performed using Stata Statistical Software, Release 11 (StataCorp 2009). The normal distribution of data was analysed using a Shapiro-Wilk normality test. A non-parametric test was employed to analyse the experiments in which some of the data did not fit a normal distribution or the sample size was lower than 8. Data were evaluated using a one-sided Wilcoxon nonparametric test to compare two groups and a two-sided Kruskal-Wallis nonparametric test to compare more than two groups. Statistical significance was set at p-values $\leq$0.05. All results are represented as median and interquartile range.

3. Results

3.1. Nanoparticle characterization

3.1.1. MSNs can load and release antibacterial compounds

The correct synthesis of the bone-targeted, coated nanoparticles was confirmed through different characterization techniques (See Supporting Information). The loading capacity was found to be 54.18±1.86 µg MX/mg MSNs and 37.88±3 µg RI/mg MSNs. We initially evaluated whether the coating could hamper premature

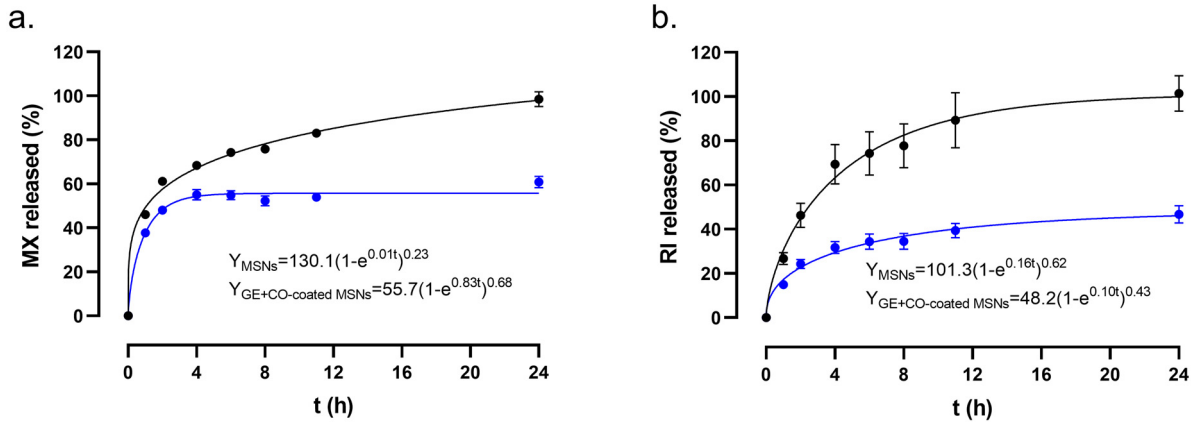

Fig. 2. Release kinetics of antibiotic-loaded nanoparticles from uncoated MSNs (black) or GE-coated (blue) MX-loaded (a) and RI-loaded (b) MSNs in absence of bacterial stimulus. Each point represents the mean of three replicates. The error bar represents the standard deviation of the replicates. The inset of each graph shows the result of the fitting of the corresponding points to a first-order release kinetics bearing a non-empirical factor δ. (For interpretation of the references to colour in this figure legend, the reader is referred to the web version of this article.)

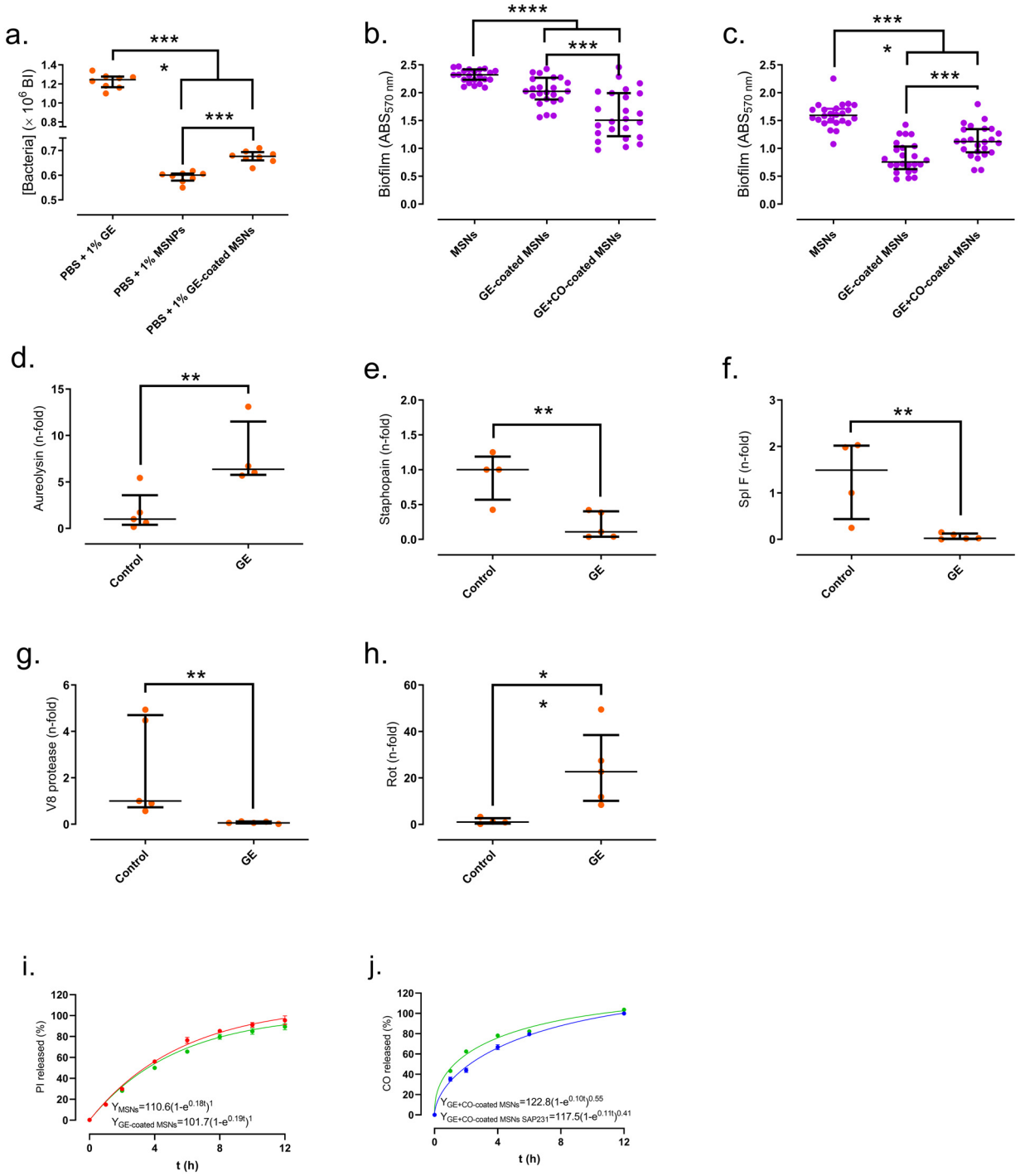

Fig. 3. Interaction between SAP231 and the different coatings evaluated in this study. (a) Concentration of SAP231 bacteria grown using gelatine (GE) as carbon source. (b) Effect of GE-coated and GE plus colistin (GE+CO)-coated MSNs on SAP231 biofilm development. (c) Effect of GE-coated and GE+CO-coated MSNs on the growth of SAP231 mature biofilm. Gene expression of SAP231 during biofilm development in presence or absence of GE: (d) aureolysin, (e) staphopain, (f) Spl F serine protease, (g) V8 protease, and (h) Rot transcriptional factor (h). Assessment of the enzyme-responsive behaviour of the nanoparticles. (i) Propidium iodide (PI) release from MSNs (red) and GE-coated-MSNs in presence of *S. aureus* (blue). (j) FITC-labelled CO release profile from GE+CO-coated MSNs (blue) and GE+CO-coated MSNs in presence of SAP231 (green). BI: bioluminescence intensity. The bars represent the median and the interquartile range (a-h). *: p-value<0.05, **: p-value<0.01, ***: p-value<0.001, ****: p-value<0.0001 for Wilcoxon test. Each point in i-j represents the mean of three replicates. The error bar represents the standard deviation of the replicates. The inset of each graph shows the result of the fitting of the corresponding points to a first-order release kinetics bearing a non-empirical factor δ. (For interpretation of the references to colour in this figure legend, the reader is referred to the web version of this article.)

antibiotic release from the mesopores in absence of any stimulus (Fig. 2). Overall, the coating was shown to reduce premature drug release in both cases, decreasing the drug release in absence of enzymatic stimulus by *ca.* 40% and *ca.* 60% for MX and RI, respectively, compared to pristine MSNs. The release data from each release experiment were fitted to a first-order kinetic model with an empirical nonideality factor (δ) (Eq. (1)) [71,72]:

$$Y = A(1 - e^{-kt})^{\delta} \quad (1)$$

With *Y* being the percentage of antibiotic released at time *t*, *A* the maximum amount of antibiotic released (in %), and *k*, the release rate constant. The equations for each release experiment are shown as insets in Fig. 2. In this model, the parameter δ can take values comprised between 0, for materials in which most of the payload release takes place at the beginning of the experiment, and 1, for materials whose release follows a pure first-order kinetic.

3.2. Microbiological studies

3.2.1. Bacteria-nanoparticle interaction

First, GE-coated MSNs were incubated with SAP231 to evaluate whether this coating could be effectively degraded by the bacterial collagenases and be employed as carbon source by this bacterium. As shown in Fig. 3a, SAP231 bioluminescence increased by 12% in the presence of GE-coated MSNs compared to pristine MSNs (p-value<0.0001). PBS supplemented with 10% of GE was used as positive control. Moreover, incubating GE-coated or GE+CO-coated MSNs with planktonic SAP231 in a biofilm development growth medium led to impaired biofilm development. Unlike MSNs, both coated groups were able to reduce the development of the SAP231 biofilm (p-value<0.0001), being especially noticeable for GE+CO-coated MSNs (p-value=0.0003 *vs*. GE-coated MSNs) (Fig. 3b). Regarding the administration of the nanoparticles onto an already grown biofilm, both coated groups demonstrated to destabilize the biofilm. In this regard, the biomass of the SAP231 mature biofilm in presence of GE-coated or GE+CO-coated MSNs was lower than in presence of pristine MSNs (p-value<0.0001), demonstrating their disaggregating features (Fig. 3c). Of note, GE-coated MSNs induced 32% more reduction of mature biofilm growth than GE+CO-coated MSNs (p-value=0.0004) (Fig. 3c).

Because GE-coated MSNs exerted the highest reduction of biomass, we analysed the expression of different *S. aureus* proteases and Rot transcriptional factor to gain insight into the antibiofilm mechanism of the GE coating (Fig. 3d-h). The expression of aureolysin (Fig. 3d) and Rot (Fig. 3h) increased 5.4-fold (p-value=0.0079) and 22.7-fold (p-value=0.0079) in presence of GE, respectively. On the contrary, the expression of staphopain, SplF, and V8 protease decreased by 89.2% (p-value=0.0079), 98.4% (p-value=0.0079), and 94.3% (p-value=0.004), respectively.

The enzymatic degradation of GE by staphylococcal collagenases was further confirmed through a release experiment. For that purpose, MSNs and GE-coated MSNs were placed with SAP231 to evaluate whether the enzyme-mediated degradation of the GE coating affected the release profile (Fig. 3i). The PI release was almost equal from MSNs and GE-coated MSNs when both were placed in presence of SAP231. Similarly, this enzymatic degradation led to slightly faster colistin release from the GE+CO-coated MSNs (Fig. 3j). PI was employed as model payload, since the antibiotics would have eliminated the bacteria, thereby stopping the secretion of bacterial proteases. Both release experiments were also fitted to the previously described kinetic model. The equations are shown in Fig. 3i-j.

3.3. Antibiotic-loaded nanoparticles inhibit and eradicate the growth of both S. aureus planktonic cell and biofilm

The antibacterial effect of the nanoparticles was evaluated by studying the MIC and MBC. For that purpose, different nanoparticles were faced against planktonic SAP231 at different concentrations. The MIC and MBC of D_6-GE+CO-coated MX-loaded MSNs were found to be 3.906 and 7.813 µg/mL, respectively. The MIC and MBC of D_6-GE+CO-coated RI-loaded MSNs were found to be <0.977 µg/mL in both cases.

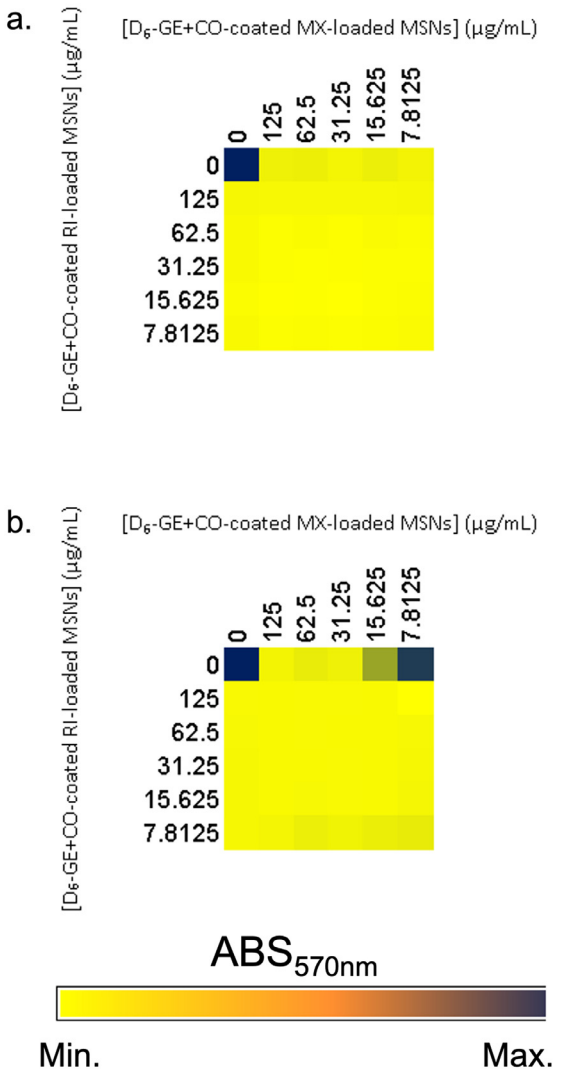

Fig. 4. Evaluation of the synergy between GE+CO-coated MX-loaded MSNs and GE+CO-coated RI-loaded MSNs for inhibiting (a) or eradicating the SAP231 biofilm (b).

The antibiofilm effect of the nanoparticles was evaluated through the analysis of the MBIC and MBEC. For that purpose, different nanoparticles were faced against a SAP231 biofilm at different concentrations. The MBIC and MBEC of D_6-GE+CO-coated MX-loaded MSNs were found to be 15,625 and 31,25 µg/mL, respectively. Analogously, the MBIC and MBEC of D_6-GE+CO-coated RI-loaded MSNs were found to be <0.977 µg/mL in both cases.

Results of the combined effect of D_6-GE+CO-coated MX-loaded MSNs and D_6-GE+CO-coated RI-loaded MSNs against SAP231 biofilm are represented in Fig. 4. As shown, D_6-GE+CO-coated MX-loaded MSNs and D_6-GE+CO-coated RI-loaded MSNs were able to inhibit the planktonic growth of SAP231 biofilm at all concentrations (Fig. 4a). All tested concentrations of D_6-GE+CO-coated RI-loaded MSNs favoured the SAP231 biofilm eradication, decreasing 4-fold the MBEC of D_6-GE+CO-coated MX-loaded MSNs alone (Fig. 4b).

3.4. Combining both groups of nanoparticles significantly reduces the infection in an in vitro osteomyelitis model

Bearing in mind the above-described results, an *in vitro* model of infected bone was developed in preparation of the *in vivo* experiment. For that purpose, three different concentrations of D_6-

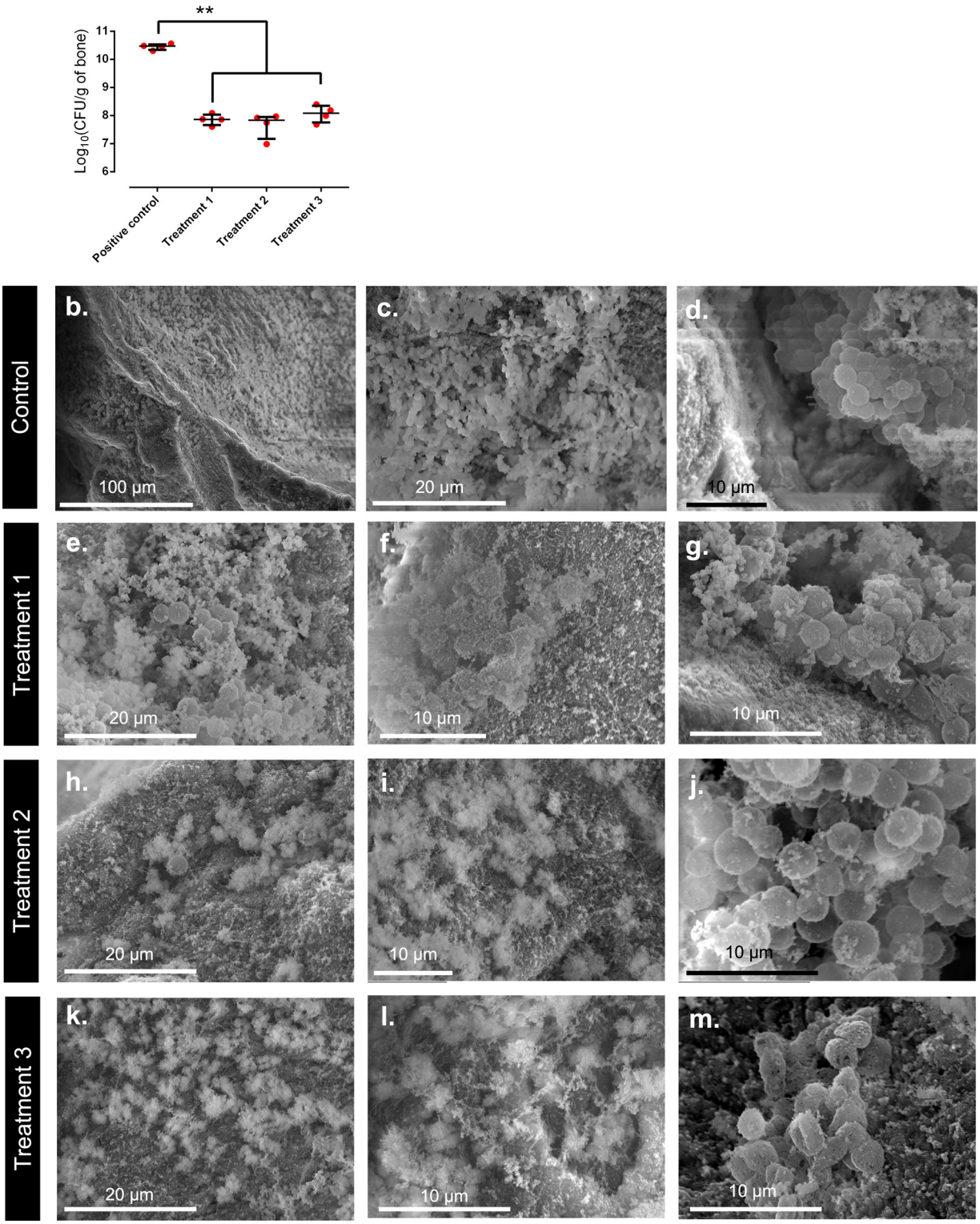

Fig. 5. SAP231 quantity per gram of trabecular bone after 24-h treatment with each condition (a) : treatment 1 (125 µg/mL of GE+CO-coated MX-loaded MSNs plus 125 µg/mL of GE+CO-coated RI-loaded MSNs), treatment 2 (125 µg/mL of GE+CO-coated MX-loaded MSNs plus 62.5 µg/mL of GE+CO-coated RI-loaded MSNs), and treatment 3 (125 µg/mL of GE+CO-coated MX-loaded MSNs plus 31.25 µg/mL of GE+CO-coated RI-loaded MSNs). The bars represent the median and the interquartile range. **: p-value<0.01 for Kruskal-Wallis's test. Representative SEM micrographs of SAP231 biofilm grown on trabecular bone after 24-h treatment. (b-d) non-treated (control), (e-g) treatment 1 (125 µg/mL of GE+CO-coated MX-loaded MSNs plus 125 µg/mL of GE+CO-coated RI-loaded MSNs), (h-j) treatment 2 (125 µg/mL of GE+CO-coated MX-loaded MSNs plus 62.5 µg/mL of GE+CO-coated RI-loaded MSNs), and (k-m) treatment 3 (125 µg/mL of GE+CO-coated MX-loaded MSNs plus 31.25 µg/mL of GE+CO-coated RI-loaded MSNs).

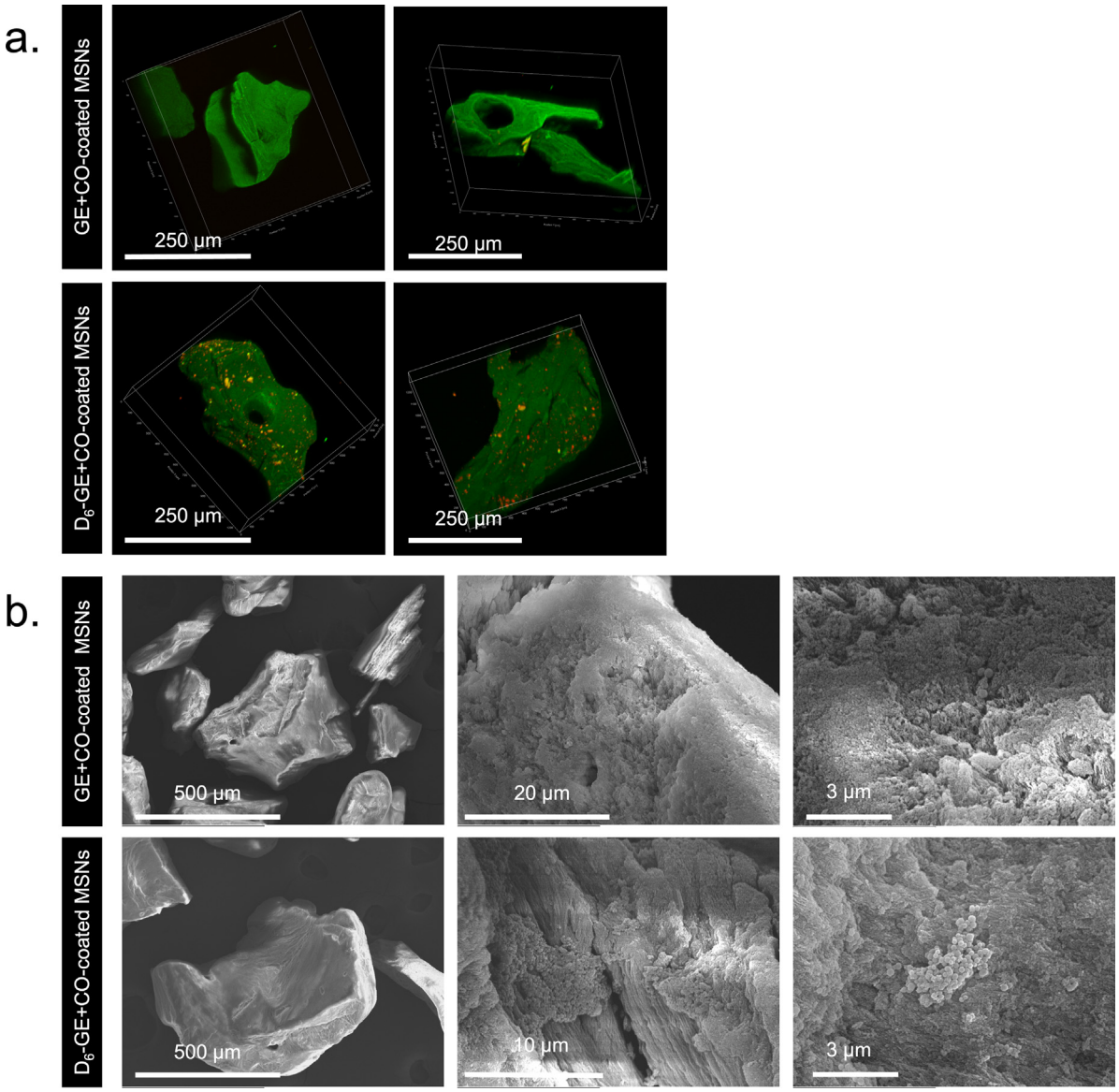

Fig. 6. Three-dimensional reconstruction (a) of trabecular bone (green) exposed to GE+CO-coated MSNs or D_6-GE+CO-coated MSNs labelled with rhodamine B (orange). The size of the bone trabeculae used is between 0.5- and 1-mm. Representative SEM micrographs of trabecular bone (b) exposed to GE+CO-coated or D_6-GE+CO-coated MSNs. (For interpretation of the references to colour in this figure legend, the reader is referred to the web version of this article.)

Table 1
Concentration of each D_6-GE+CO-coated antibiotic-loaded MSNs in each treatment. MX: moxifloxacin. RI: rifampicin.

Treatment	D_6-GE+CO-coated MX-loaded MSNs (µg/mL)	D_6-GE+CO-coated RI-loaded MSNs (µg/mL)
1		125
2	125	62.5
3		31.25

GE+CO-coated MX-loaded MSNs plus D_6-GE+CO-coated RI-loaded MSNs were chosen against a SAP231 mature biofilm grown on the trabecular bone (Table 1).

As observed in Fig. 5a, all conditions were able to reduce by 99.7% the bacterial viability of the SAP231 biofilm (p-value=0.005). Considering these results, the intermediate concentration of D_6-GE+CO-coated RI-loaded MSNs (62.5 µg/mL) was chosen for the following experiments.

To further support these numerical results, representative SEM micrographs from each treatment were taken (Fig. 5b-m). The non-treated SAP231 biofilm showed microcolonies adhered on the trabecular bone pieces composed of cocci 0.5 to 0.8 µm in diameter (Fig. 5b-d). All treated SAP231 biofilms showed similar appearance: microcolonies with clumps of nanoparticles adhered to their surfaces and covered with open polymeric skeins (Fig. 5e-m). At high magnifications, the damage inflicted by MX and RI was reflected in the significant structural damage to the wall of the staphylococci imaged (Fig. 5m).

3.5. D_6-GE+CO-coated antibiotics-loaded MSNs target bone tissue in vitro and prevent the development of S. aureus biofilm

The targeting ability towards bone of the D_6-GE+CO-coated MSNs was evaluated through confocal laser-scanning microscope and SEM. The three-dimensional reconstructions from the confocal laser-scanning microscope demonstrated that only D_6-GE+CO-coated MSNs were able to attach to the bone surface (Fig. 6a). In this regard, D_6-GE+CO-coated MSNs adhered irregularly, forming

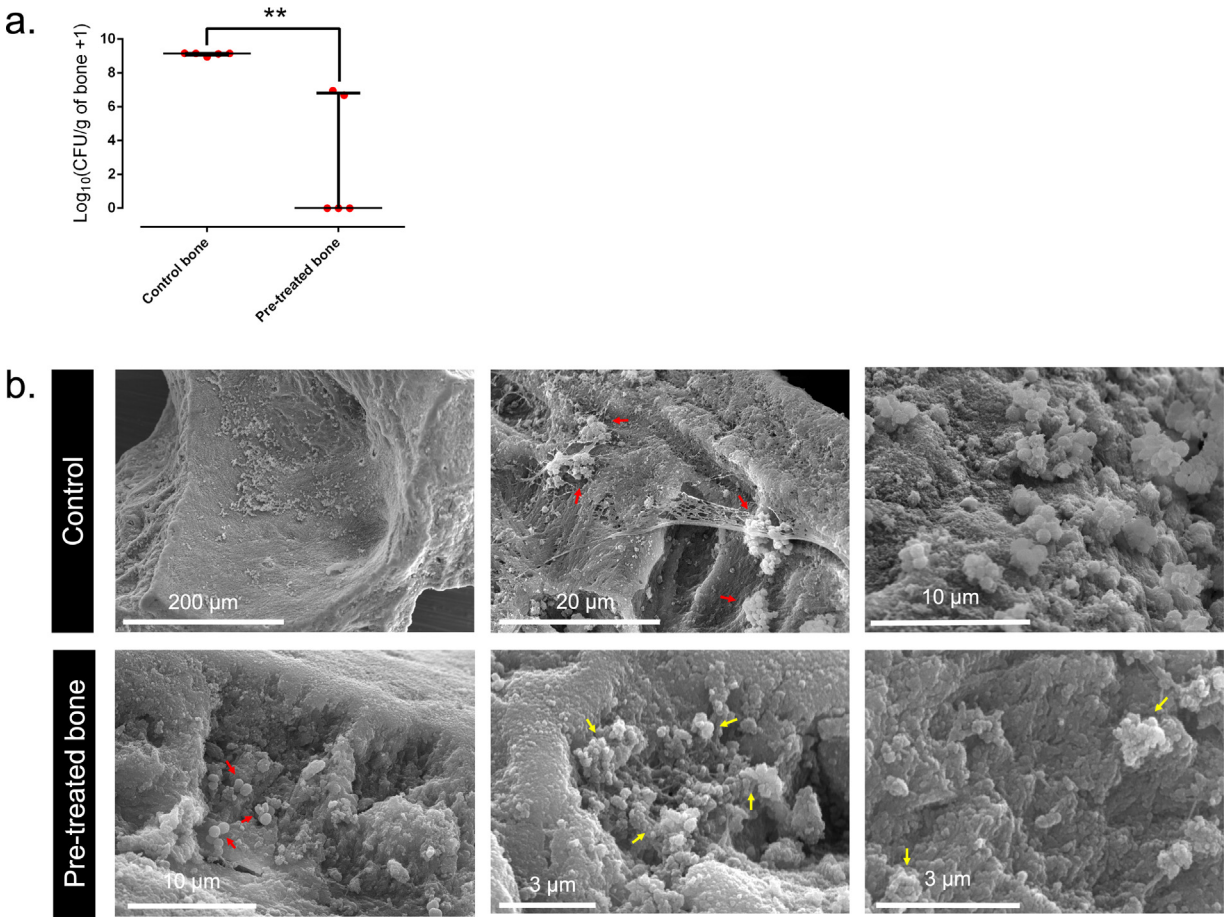

Fig. 7. SAP231 quantity per gram of trabecular bone grown on trabecular bone pre-treated with a mixture of D_6-GE+CO-coated MX-loaded MSNs and D_6-GE+CO-coated RI-loaded MSNs (a). The bars represent the median and the interquartile range. **: p-value<0.01 for Wilcoxon test. Representative SEM micrographs of SAP231 biofilm grown on trabecular bone pre-treated with a mixture of D_6-GE+CO-coated MX-loaded MSNs and D_6-GE+CO-coated RI-loaded MSNs (b). The yellow, green, blue, and red bars represent 200, 20,10, and 3 µm, respectively. Red arrows indicate staphylococcal cells or aggregates. Yellow arrows point out D_6-GE+CO-coated antibiotic-loaded MSNs. (For interpretation of the references to colour in this figure legend, the reader is referred to the web version of this article.)

small clusters of nanoparticles on the surface, ranging from 3 to 15-20 µm (Fig. 6b).

Furthermore, pre-treating the bone with a 1:1 mixture of D_6-GE+CO-coated MX-loaded MSNs and D_6-GE+CO-coated RI-loaded MSNs led to almost complete inhibition (99.1-100%) of SAP231 biofilm development on the bone surface (Fig. 7a). These numerical results were further supported by representative SEM micrographs taken from each condition (Fig. 7b). The SAP231 biofilm grown on the non-pre-treated bone showed abundant exopolysaccharide matrix (Fig. 7b, control) and numerous microcolonies adhered on trabecular bone pieces composed of cocci 0.5 to 0.8 µm in diameter (Fig. 7b, red arrows). On other hand, only scarce and isolated cocci could be observed on the nanoparticle-pre-treated bone (Fig. 7b, red arrows). As observed above, D_6-GE+CO-coated MSNs formed clusters on the bone (Fig. 7b, yellow arrows).

3.6. The nanosystems are biocompatible on bone-related cells

The biocompatibility of D_6-GE+CO-coated antibiotics-loaded MSNs was evaluated on bone-related cells (Fig. 8). The treatment was found to be non-cytotoxic over time for osteoblasts and macrophages (Fig. 8a, c), whereas some cytotoxicity over time could be observed for osteoclasts (Fig. 8b) during the first 72 h of exposure. Similarly, D_6-GE+CO-coated antibiotic-loaded MSNs had moderate impact on the cell metabolic activity of osteoclasts and macrophages (Fig. 8e-f), whereas that of osteoblasts showed a slight but significant increase of 11% (Fig. 8d).

3.7. In vivo *studies*

3.7.1. D_6-GE+CO-coated MSNs target bone tissue in vivo

Having confirmed *in vitro* that D_6-GE+CO-coated MSNs outperformed the non-functionalized MSNs in terms of bone targeting, only the former was evaluated *in vivo* to minimize the number of animals to be employed and comply with the three R's rule. The results obtained are shown in Fig. 9. The semiquantitative analysis clearly showed the presence of the D_6-GE+CO-coated MSNs in the four portions of the femur 5 min after the intraosseous injection. Overall, slightly lower but comparable fluorescence intensity was measured in the four portions of the femur after 24 h (Fig. 9). At 5 min, the highest concentrations of D_6-GE+CO-coated MSNs were detected in the epiphyses (Fig. 9b, portions 1 and 4), decreasing after 24 h from the site of injection in the distal epiphysis (Fig. 9b, portion 4) to the proximal epiphysis (Fig. 9b, portion 1). Interestingly, no differences in concentration of D_6-GE+CO-coated MSNs were observed between 5 min and 24 h in the distal epiphysis (Fig. 9b, portion 4).

Overall, the liver and kidneys of the two animals that received the intraosseous D_6-GE+CO-coated MSNs injection showed no histological alteration, whilst the spleen showed just a mild type of expansion of red pulp with a depletion of white pulp (Fig. S4a).

3.7.2. *Combining both nanosystems reduces the infection* in vivo

All rabbits recovered from the surgery. The weight of the positive control remained unaffected over time (R^2=0.05624; p-

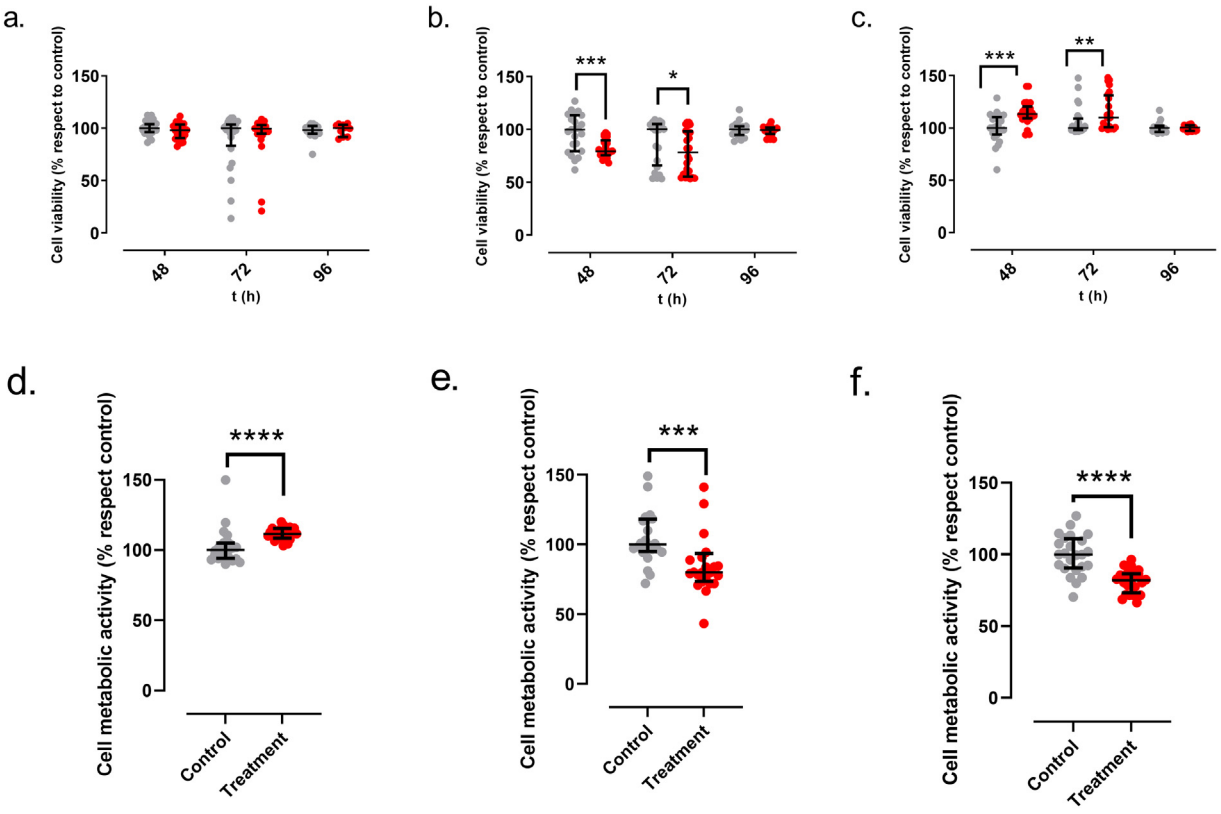

Fig. 8. Cytotoxicity of 125 µg/mL of D_6-GE+CO-coated MX-loaded MSNs plus 62.5 µg/mL of D_6-GE+CO-coated RI-loaded MSNs (red) on MC3T3-E1 osteoblasts (a), RAW264.7 osteoclasts (b), and RAW264.7 macrophages (c). Cell proliferation of MC3T3-E1 osteoblasts (d), RAW264.7 osteoclasts (e), and RAW264.7 macrophages (f) in presence of 125 µg/mL of D_6-GE+CO-coated MX-loaded MSNs plus 62.5 µg/mL of D_6-GE+CO-coated RI-loaded MSNs. *: p-value<0.05, **: p-value<0.01, ***: p-value<0.001 for Wilcoxon test.****: p-value<0.0001 for Wilcoxon test.

value=0.2244) (Fig. 10a), whereas that of the treated group increased over time (R^2=0.1816; p-value=0.0237) by *ca.* 70 mg per day (Fig. 10a). Though some rabbits showed fever (>40 °C) (Fig. 10b, yellow area), overall temperature remained constant over time (R^2=0.0991, p-value=0.1028 for the positive control group and R^2=0.001365, p-value=0.8519 for the treated group). Regarding the antibacterial effect, the selected dose reduced the concentration of colony-forming units per gram of femur by 91.4% after just one dose (p-value=0.0364) (Fig. 10c).

The pathological analysis of the kidneys of all animals (treated and untreated) revealed no histological alteration. Regarding the spleens, both untreated and treated rabbits showed one type of expansion of red pulp with depletion of white pulp (Fig. S4). Out of the untreated animals, 2, 3 and 2 rabbits showed mild, moderate, and severe expansion of red pulp with depletion of white pulp, respectively. Among the treated rabbits, 1, 4 and 2 animals showed mild, moderate, and severe expansion of red pulp with depletion of white pulp, respectively.

The liver of three out of seven untreated rabbits was normal (Fig. S5a-b), while three of them showed mild portal (Fig. S5c-d), periportal or lobular inflammatory infiltrates (Fig. S5e-f), and one of them showed hepatic necrosis with marked sinusoidal congestion. Among the treated rabbits, the liver of one of them was normal; five out of seven showed mild, periportal and/or lobular inflammation of the liver; and only one showed significant presence of eosinophils in the infiltrates.

The histology of the condyle and the joint of each group is shown in Fig. S6. The condyle of two animals from both groups was normal (Fig. S6a-b). Five rabbits from the untreated group showed mild or moderate bone inflammation (Fig. S6c-d), and two showed a bone abscess (Fig. S6e-f). Two rabbits from the treated group showed mild bone inflammation, one showed a bone abscess, and one showed an intraarticular abscess. Two animals from the treated group showed mild inflammation of the cartilage of the femoral condyle (Fig. S6g-h).

4. Discussion

In this study, we demonstrate the feasibility of using a combination of D_6-GE+CO-coated nanoparticles loaded with either MX or RI to treat bone infections caused by MRSA, showing no cytotoxicity on osteoblast and macrophages *in vitro*, and absence of organ damage *in vivo* upon intraosseous administration.

MSNs were synthesized following a modification of the Stöber method, using CTAB as structure directing agent and TEOS as silica source. Following the synthesis, the surfactant was removed from the pores using an ethanolic solution of NH_4NO_3, yielding MSNs with empty pores ready to be filled with the antibiotics. The nanoparticles were sequentially modified to finally yield the bone-targeted, GE+CO-coated MSNs, as demonstrated by the physicochemical characterization (See Supporting Information).

The release experiment carried out for each antibiotic-loaded nanoparticles was conceived to demonstrate that the coating was able to minimize and slow down premature release of the drugs from the mesopores in absence of bacterial enzymes, compared to the pristine MSNs (Fig. 2). Both plots show a biphasic behaviour: an initial phase where a high amount of cargo is rapidly released, and a second one where the release is more sustained. The initial phase would be related with the drug that is not confined within the pores, but on the outer section of the pores/on the surface. These molecules are the first to be released and constitute what is referred to as “premature drug release”. On the other hand, the second phase is ascribed to the molecules that are progressively desorbed from the inner part of the pores. In view of the results,

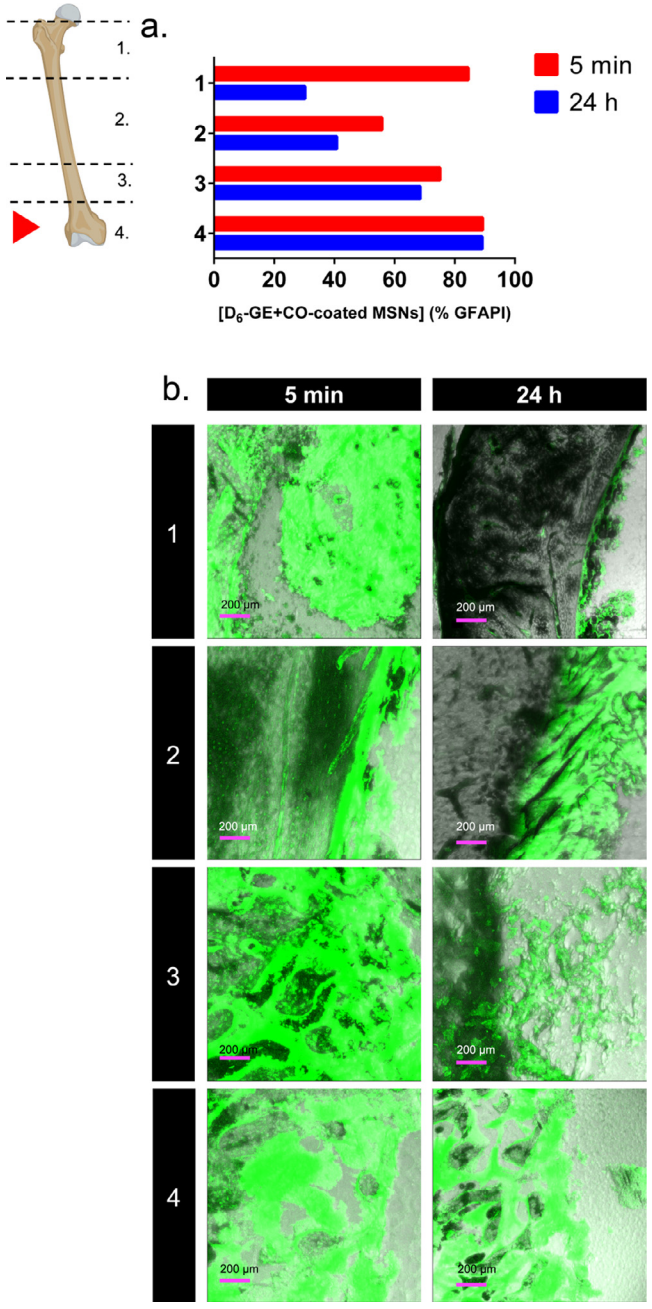

Fig. 9. *In vivo* affinity toward bone of the D_6-GE+CO-coated MSNs. (a) Percentage of green fluorescence area per image (%GFAPI) at 5 min (red) and 24 h (blue) in the different portions of the femur (1,2,3,4). The red arrow represents the anatomical site of injection. (b) Representative images of the different portions of the femur at different time points after nanoparticle administration. Dark grey and black represent the bone. Green denotes D_6-GE+CO-coated MSNs labelled with fluorescein isothiocyanate. (For interpretation of the references to colour in this figure legend, the reader is referred to the web version of this article.)

it was shown that the GE coating could minimize such premature drug release. Hence, the better part of the drug release would take place in presence of bacterial enzymes, *i.e.*, localized and restricted to the infected area. A major implication of these findings is that those nanoparticles unable to remain attached to the bone upon the intraosseous administration would keep most of the loaded drugs confined within the pores, thereby minimizing the presence of free drug in the organism and reducing potential side effects. The release of the different antibiotics in absence of stimulus was further analysed by fitting the data to a modified first-order kinetic model. According to Fig. 2a, the δ values estimated for the MX-loaded nanoparticles were 0.23 and 0.68 for pristine and coated MSNs, respectively. These values would account for the faster release observed for the MX-loaded pristine MSNs at the beginning of the experiment. When the RI-loaded nanoparticles were fitted to the model, any of them was close to 0, which would account for the slower release observed in both cases, compared to the MX-loaded pristine nanoparticles. This behaviour would be likely ascribed to the different electrostatic interactions of the drugs with the silica matrix as well as to the hydrophilicity/hydrophobicity nature of each antibiotic.

The rationale behind the selection of GE as coating for the nanoparticles relied on the enzyme-mediated degradation of this biocompatible component. In this regard, staphylococci can secrete 3 families of proteases: metalloproteases, cysteine proteases, and serine proteases [73]. Hence, these proteases would degrade the GE coating, accelerating the antibiotic delivery from the GE+CO-coated MSNs on the infected bone, as shown through different approaches in Fig. 3. Indeed, the cargo release from GE+CO-coated MSNs in presence of bacteria matched that of pristine MSNs, unlike it happened in absence of enzymatic stimulus (Fig. 2).

The fact that GE+CO-coated MSNs impaired the biofilm development (Fig. 3b) and destabilized the already grown mature biofilm (Fig. 3c) have relevant consequences. First, destabilizing the mature biofilm would trigger the release of planktonic bacteria in an infected bone, which are more susceptible to antibiotics. On the other hand, the preventive antibiofilm effect of the nanosystem would avoid the reinfection of clean areas of the infected bone. This anti-biofilm effect is consistent with a previous work that described the CO ability to destabilize the structure of the *S. aureus* biofilm matrix [29]. Interestingly, our findings demonstrated that the antibiofilm effect observed at short incubation times was rather ascribed to the nature of the GE coating. In this regard, *S. aureus* is known to produce 12 different proteases: one metalloprotease (aureolysin), two cysteine proteases (staphopains A and B), and nine different serine proteases. These serine proteases include V8 protease, six serine protease-like proteins (A-F), and two exfoliative toxins (A and B) [73]. In consequence, the destabilization of the *S. aureus* biofilm might stem from the increase of repressor of toxins (Rot) and aureolysin and gene expression (Fig. 3d, h). The Rot protein is a DNA-binding transcriptional regulator that directly binds protease gene promoters and inhibits their transcription [49], which would explain the reduced levels of some proteases like staphopain A, SplF and V8 protease (Fig. 3e-g). Aureolysin, a single-chain metalloprotease that binds one zinc and three calcium ions [74], has been shown to limit the biofilm formation of both MRSA and methicillin-susceptible *S. aureus* [75]. Interestingly, though some authors have asserted that Rot protein inhibit all proteases in general [49], according to our results the presence of GE in the GE+CO coating could repress the expression of other proteases (e.g., staphopain A, SplF and V8 protease) via the Rot protein while preferably favouring the expression of aureolysin. The regulation of these proteases has relevant implications. In this regard, it has been recently reported that MSNs can be functionalized with enzymes to target *S. aureus* biofilms and disperse them [76]. However, enzymes are labile structures that can suffer rapid degradation in living tissues, and even the anchoring method can compromise the enzymatic activity [77]. Nonetheless, incorporating these easy-to-perform gelatine coating would abrogate the need to deal with those issues, while promoting the active dispersal of the biofilm by the staphylococci themselves.

The route of administration (local injection) stems from a main characteristic of osteomyelitis, which is the presence of congested or thrombosed blood vessels [78]. This feature seriously compromises the vascularization of infected bone and makes it impossible to treat this infection systemically without previous surgery. Be-

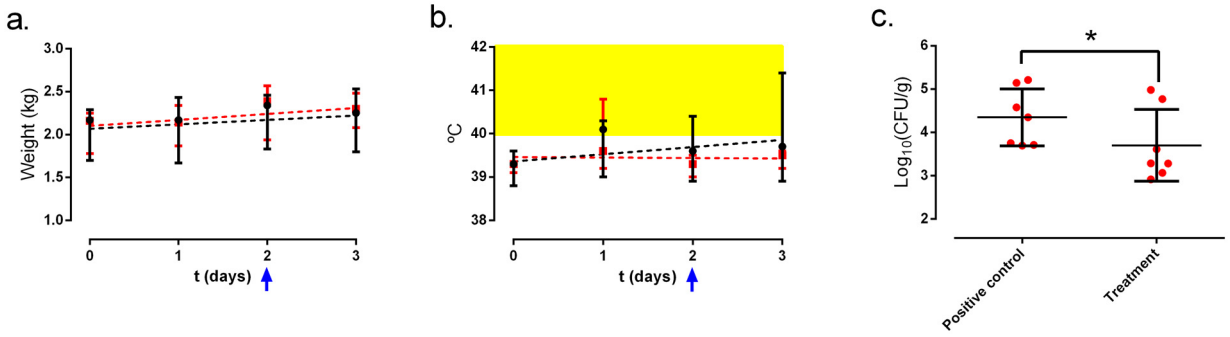

Fig. 10. Rabbit model of osteomyelitis caused by SAP231. (a) Rabbit weight and (b) temperature over time. Untreated (positive control) and treated (treatment) groups are represented in black and red, respectively. The yellow area represents fever in the rabbits. (c) SAP231 quantity per gram of femur. The bars represent the median and interquartile range. *: p-value<0.05. Blue arrow indicates the day of treatment in the treated group. (For interpretation of the references to colour in this figure legend, the reader is referred to the web version of this article.)

cause nanoparticles might be rapidly cleared from the site of injection, they were modified with the D_6 peptide, a peptide that shows high affinity toward hydroxyapatite, which is a major component of bone [46]. As expected, D_6-Ge+CO-coated MSNs outperformed the bone targeting ability of pristine MSNs in the *in vitro* model of bone (Fig. 5), reason why the former was selected as best candidate and was employed for the subsequent experiments.

In light of the resulting MBIC and MBEC, each nanosystem could be individually applied to the treatment for MRSA biofilm, as recommended by other authors [79,80]. Nevertheless, it is important to highlight that RI monotherapy is contraindicated for staphylococcal infections, being always used in combination with other compounds [81–83]. Hence, to maximize the efficacy of the treatment and comply with the clinical management, it was evaluated whether there was synergy against SAP231 biofilm between both nanosystems. In this regard, it was found that both nanosystems presented at least a cooperative effect for inhibiting the growth of the SAP231 biofilm, as well as for eradicating it (Fig. 4). In this sense, using the RI-loaded nanoparticles combined with the MX-loaded ones clearly improved the eradication capacity of the latter, as the required dose of MX-loaded MSNs decreased four times when the combination was employed.

The antibacterial efficacy of D_6-GE+CO-coated antibiotic-loaded MSNs was further evaluated using an *in vitro* model of MRSA biofilm grown in wound-like medium on bovine trabecular bone in which all tested conditions removed more than 99% of the bacterial load. This experiment allowed to optimize the therapeutic conditions for the subsequent *in vivo* experiments (125 μg/mL for MX-loaded and 62.5 μg/mL for RI-loaded nanosystems). In addition to showing the infection-preventing capacity, these nanoparticles proved to prevent the appearance of new infected areas (Fig. 7), indicating again that this treatment would be useful to prevent bacterial colonization of intact bone of the infected bone foci.

Osteomyelitis provokes progressive inflammatory tissue destruction, which in the end induces marked local bone resorption and proximal abnormal bone formation in the infected bone. Excluding bacteria, this process is mainly regulated by three main types of cells, namely osteoblasts/osteocytes, osteoclast and macrophages [84], whose cell viability would remained mostly unaffected in the presence of nanoparticles (Fig. 8b). The cytocompatibility of gelatine-coating is well-known [85–89]. On the other hand, the observed osteoblastic metabolic activity (Fig. 8d-f) is coherent with previous studies that described the osteoblast-stimulant effect of the GE [90–93], since collagen can trigger the recruitment of osteoblasts during bone remodelling [94]. Conversely, it has been shown that it might have some negative effects on the osteoclastic proliferation [95], which is supported by our results of cytotoxicity over time and metabolic activity. In addition, the reduced macrophagic metabolic activity could be consequence of the antibiotics used. In this sense, CO inhibits cell metabolic activity in general [96], MX presents antiproliferative effect on certain cells [97], and RI is known to induce depression of the immune response and reduction of phagocytic activity [98].

Having identified *in vitro* the best candidate in terms of both bone-targeting and antibacterial features, its performance was evaluated *in vivo*. First, D_6-GE+CO-coated MSNs were intraosseously injected in the femur of the rabbits, showing nanoparticle attachment to the cancellous bone of the bone marrow for at least 24 h, assuring enough time for the antibiotics to be locally released. Of note, it was found that the adherence of the functionalized nanoparticles at 5 min increased with the amount of cancellous bone in the femur. Conversely, it was observed that the concentration of nanosystem adhered to the bone at 24 h increased when the distance of the observed femur portion to the injection site decreased. These findings are consistent with the histological composition of the femur, since the surface associated to cancellous marrow is higher in the epiphysis than in the diaphysis [99]. Regarding the elimination of the nanoparticles, these foreign bodies are normally captured by the reticuloendothelial system, which is located in some organs such as the spleen, liver, kidney and lungs [100]. In this regard, the rabbits that received the intravenous injection of D_6-GE+CO-coated MSNs showed mild expansion of red pulp with depletion of white pulp type. These pathological findings would confirm that the nanoparticles that were unable to remain attached to the bone were cleared by the reticuloendothelial system from the spleen. Similar findings were found by a previous study that reported red pulp expansion and relative white pulp shrinkage in the spleen of mice treated with a high dose of MSNs [101].

The D_6-GE+CO-coated antibiotic-loaded MSNs treatment was able to reduce the *S. aureus* concentration more than 92% in the infected rabbit femurs in just 24 h with just one dose, highlighting the antimicrobial efficacy of the bone-targeted nanoparticles (Fig. 10c). In this regard, should this nanosystem be translated into the clinic, the patients could benefit from the periodic intraosseous application of this treatment. This treatment regime would guarantee high and sustained local drug delivery, which would progressively diminish the bacterial load after each dose. In consequence, this nanosystem could be used as intraosseous treatment of infected bones. It must be considered that the results derived from the *in vivo* model are the result of a single dose. However, the potential patients that would receive this treatment could be injected periodic doses, increasingly reducing the bacterial load after each of them.

The pathological findings also supported the microbiological results. The livers of both groups showed mild central perivenous inflammation and minimal lobular hepatitis accompanied by an inflammatory infiltrate, which is indicative of a bacterial in-

fectious process taking place [102]. This pathological finding was slightly more common in the animals treated with D6-GE+CO-coated MSNs. The spleen of the untreated rabbits showed mild or moderate expansion of red pulp with depletion of white pulp type, which would be ascribed to the splenic detection of the haemolysis caused by *S. aureus* [103,104]. Again, the infected group that received an intravenous injection of D6-GE+CO-coated MSNs showed animals with moderate or severe expansion of red pulp with depletion of white pulp type. This may be consequence of: (1) the splenic recruitment of the injected nanoparticles unable to attach to the bone, and (2) the uptake of remains of the bacterial lysis or dead S. aureus bacteria detached from the treated biofilm, since the liver and spleen are the two organs able to filter bacteria from blood [111].

5. Conclusions

In this work, we have engineered bone-targeted MSNs against MRSA osteomyelitis. Two sets of nanoparticles have been prepared, each of them carrying a clinically relevant antibiotic. To prevent premature drug release, the nanoparticles have been functionalized with a biocompatible coating containing enzymatically degradable gelatine and CO, an antibiotic with biofilm-disaggregating features. The nanosystem demonstrated high affinity toward bone tissue thanks to the bone targeting hexapeptide and marked synergistic antibacterial effect thanks to the combined used of MX and RI. The combined treatment could reduce and locally prevent *in vitro* the infection developed on a trabecular bone and showed pronounced antibacterial efficacy *in vivo* against a MRSA-provoked osteomyelitis. Furthermore, D_6-GE+CO-coated antibiotics-loaded MSNs were shown to be highly biocompatible, with only moderate cytotoxic and antiproliferative effect on osteoclasts. Considering these results, combining these bone-targeted antibacterial nanocarriers could help to overcome the pitfalls of current treatments for bone infections caused by methicillin-resistant staphylococci, as well as to minimize the increasing global concern of antimicrobial resistance.

Declaration of Competing Interest

The authors declare that they have no known competing financial interests or personal relationships that could have appeared to influence the work reported in this paper.

CRediT authorship contribution statement

J.J. Aguilera-Correa: Conceptualization, Methodology, Software, Validation, Formal analysis, Investigation, Data curation, Writing – original draft, Writing – review & editing, Visualization. **M. Gisbert-Garzarán:** Conceptualization, Validation, Formal analysis, Investigation, Data curation, Writing – original draft, Writing – review & editing, Visualization. **A. Mediero:** Investigation, Data curation, Writing – original draft, Writing – review & editing, Visualization. **M.J. Fernández-Aceñero:** Investigation, Data curation, Writing – original draft, Writing – review & editing. **D. de-Pablo-Velasco:** Investigation, Writing – review & editing. **D. Lozano:** Investigation, Data curation, Writing – original draft, Writing – review & editing. **J. Esteban:** Validation, Investigation, Writing – review & editing, Visualization, Supervision. **M. Vallet-Regí:** Validation, Investigation, Resources, Writing – review & editing, Visualization, Supervision, Project administration, Funding acquisition.

Acknowledgements

The authors acknowledge the financial support from the European Research Council through ERC-2015-AdG-694160 (VERDI) grant. AM is funded by grants from Instituto de Salud Carlos III through the “Miguel Servet” program (CP15/00053). We also wish to acknowledge Roger Plaut from United States Food & Drugs Administration for providing us the bioluminescent MRSA (SAP231), María del Mar González García-Parreño from IIS- Fundación Jimenez Diaz for her help with the use of the confocal laser-scanning microscope, and Beatriz Toirac-Chávez and Antonia Jiménez-Morales from Carlos III University of Madrid for manufacturing the Ti-6Al-4V implants used in the *in vivo* model of this study. Parts of this work were previously presented at the 32nd European Congress of Clinical Microbiology and Infectious Diseases, and 25th Spanish Congress of Clinical Microbiology and Infectious Diseases. Graphical abstract, Scheme 1, and some icons from Figs. S4, S5 and S6 have been created with BioRender.com.

Supplementary materials

Supplementary material associated with this article can be found, in the online version, at doi:10.1016/j.actbio.2022.10.039.

References

[1] M.C. Birt, D.W. Anderson, E. Bruce Toby, J. Wang, Osteomyelitis: Recent advances in pathophysiology and therapeutic strategies, J. Orthop. 14 (2017) 45–52, doi:10.1016/j.jor.2016.10.004.
[2] H.M. Kremers, M.E. Nwojo, J.E. Ransom, C.M. Wood-Wentz, L.J. Melton, P.M. Huddleston, Trends in the epidemiology of osteomyelitis: a population-based study, 1969 to 2009, J. Bone. Joint Surg. Am. 97 (2015) 837–845, doi:10.2106/JBJS.N.01350.
[3] V. Silago, M.F. Mushi, B.A. Remi, A. Mwayi, S. Swetala, C.I. Mtemisika, S.E. Mshana, Methicillin resistant Staphylococcus aureus causing osteomyelitis in a tertiary hospital, Mwanza, Tanzania, J. Orthop. Surg. Res. 15 (2020) 95, doi:10.1186/s13018-020-01618-5.
[4] N.A. Turner, B.K. Sharma-Kuinkel, S.A. Maskarinec, E.M. Eichenberger, P.P. Shah, M. Carugati, T.L. Holland, V.G. Fowler, Methicillin-resistant Staphylococcus aureus: an overview of basic and clinical research, Nat. Rev. Microbiol. 17 (2019) 203–218, doi:10.1038/s41579-018-0147-4.
[5] World Health Organization, Global Antimicrobial Resistance and Use Surveillance System (GLASS) Report: 2021, World Health Organization, Geneva, 2021. https://apps.who.int/iris/handle/10665/341666 (accessed October 4, 2021).
[6] S. Singh, R. Malhotra, P. Grover, R. Bansal, S. Galhotra, R. Kaur, N. Jindal, Antimicrobial resistance profile of Methicillin-resistant Staphylococcus aureus colonizing the anterior nares of health-care workers and outpatients attending the remotely located tertiary care hospital of North India, J. Lab. Physicians 9 (2017) 317–321, doi:10.4103/JLP.JLP_8_17.
[7] K.L. de Mesy Bentley, R. Trombetta, K. Nishitani, S.N. Bello-Irizarry, M. Ninomiya, L. Zhang, H.L. Chung, J.L. McGrath, J.L. Daiss, H.A. Awad, S.L. Kates, E.M. Schwarz, Evidence of Staphylococcus aureus deformation, proliferation, and migration in canaliculi of live cortical bone in murine models of osteomyelitis, J. Bone Miner. Res. 32 (2017) 985–990, doi:10.1002/jbmr.3055.
[8] K.L. de Mesy Bentley, A. MacDonald, E.M. Schwarz, I. Oh, Chronic Osteomyelitis with Staphylococcus aureus deformation in submicron canaliculi of osteocytes: a case report, JBJS Case Connect. 8 (2018) e8, doi:10.2106/JBJS.CC.17.00154.
[9] R. Sunyer, V. Conte, J. Escribano, A. Elosegui-Artola, A. Labernadie, L. Valon, D. Navajas, J.M. García-Aznar, J.J. Muñoz, P. Roca-Cusachs, X. Trepat, Collective cell durotaxis emerges from long-range intercellular force transmission, Science 353 (2016) 1157–1161, doi:10.1126/science.aaf7119.
[10] E.A. Masters, R.P. Trombetta, K.L. de Mesy Bentley, B.F. Boyce, A.L. Gill, S.R. Gill, K. Nishitani, M. Ishikawa, Y. Morita, H. Ito, S.N. Bello-Irizarry, M. Ninomiya, J.D. Brodell, C.C. Lee, S.P. Hao, I. Oh, C. Xie, H.A. Awad, J.L. Daiss, J.R. Owen, S.L. Kates, E.M. Schwarz, G. Muthukrishnan, Evolving concepts in bone infection: redefining “biofilm”, “acute vs. chronic osteomyelitis”, “the immune proteome” and “local antibiotic therapy, Bone Res. 7 (2019) 20, doi:10.1038/s41413-019-0061-z.
[11] E. Garcia del Pozo, J. Collazos, J.A. Carton, D. Camporro, V. Asensi, Factors predictive of relapse in adult bacterial osteomyelitis of long bones, BMC Infect. Dis. 18 (2018) 635, doi:10.1186/s12879-018-3550-6.
[12] D.H. Libraty, C. Patkar, B. Torres, Staphylococcus aureus reactivation osteomyelitis after 75 years, N. Engl. J. Med. 366 (2012) 481–482, doi:10.1056/NEJMc1111493.
[13] J.M. Fritz, J.R. McDonald, Osteomyelitis: approach to diagnosis and treatment, Phys. Sportsmed. 36 (2008) nihpa116823, doi:10.3810/psm.2008.12.11.
[14] H. Ragelle, F. Danhier, V. Préat, R. Langer, D.G. Anderson, Nanoparticle-based drug delivery systems: a commercial and regulatory outlook as the field matures, Expert Opin. Drug Deliv. 14 (2017) 851–864, doi:10.1080/17425247.2016.1244187.
[15] M. Gisbert-Garzarán, M. Manzano, M. Vallet-Regí, Mesoporous silica nanoparticles for the treatment of complex bone diseases: bone cancer, bone

infection and osteoporosis, Pharmaceutics 12 (2020) 83, doi:10.3390/pharmaceutics12010083.
[16] M. Vallet-Regi, A. Rámila, R.P. del Real, J. Pérez-Pariente, A new property of MCM-41: drug delivery system, Chem. Mater. 13 (2001) 308–311, doi:10.1021/cm0011559.
[17] M. Manzano, M. Vallet-Regí, Mesoporous silica nanoparticles for drug delivery, Adv. Funct. Mater. 30 (2020) 1902634, doi:10.1002/adfm.201902634.
[18] J. Lu, M. Liong, Z. Li, J.I. Zink, F. Tamanoi, Biocompatibility, biodistribution, and drug-delivery efficiency of mesoporous silica nanoparticles for cancer therapy in animals, Small 6 (2010) 1794–1805, doi:10.1002/smll.201000538.
[19] J.L. Vivero-Escoto, I.I. Slowing, B.G. Trewyn, V.S.-Y. Lin, Mesoporous silica nanoparticles for intracellular controlled drug delivery, Small 6 (2010) 1952–1967, doi:10.1002/smll.200901789.
[20] Z. Kuang, G. Dai, R. Wan, D. Zhang, C. Zhao, C. Chen, J. Li, H. Gu, W. Huang, Osteogenic and antibacterial dual functions of a novel levofloxacin loaded mesoporous silica microspheres/nano-hydroxyapatite/polyurethane composite scaffold, Genes Dis. 8 (2021) 193–202, doi:10.1016/j.gendis.2019.09.014.
[21] Q. Wang, C. Chen, W. Liu, X. He, N. Zhou, D. Zhang, H. Gu, J. Li, J. Jiang, W. Huang, Levofloxacin loaded mesoporous silica microspheres/nano-hydroxyapatite/polyurethane composite scaffold for the treatment of chronic osteomyelitis with bone defects, Sci. Rep. 7 (2017) 41808, doi:10.1038/srep41808.
[22] B. Nie, S. Huo, X. Qu, J. Guo, X. Liu, Q. Hong, Y. Wang, J. Yang, B. Yue, Bone infection site targeting nanoparticle-antibiotics delivery vehicle to enhance treatment efficacy of orthopedic implant related infection, Bioact. Mater. (2022), doi:10.1016/j.bioactmat.2022.02.003.
[23] Y.J. Lee, S. Sadigh, K. Mankad, N. Kapse, G. Rajeswaran, The imaging of osteomyelitis, Quant. Imaging Med. Surg. 6 (2016) 184–198, doi:10.21037/qims.2016.04.01.
[24] M. Gisbert-Garzaran, D. Lozano, M. Vallet-Regí, M. Manzano, Self-immolative polymers as novel pH-responsive gate keepers for drug delivery, RSC Adv. 7 (2017) 132–136, doi:10.1039/C6RA26771H.
[25] M. Martínez-Carmona, D. Lozano, M. Colilla, M. Vallet-Regí, Selective topotecan delivery to cancer cells by targeted pH-sensitive mesoporous silica nanoparticles, RSC Adv. 6 (2016) 50923–50932, doi:10.1039/C6RA07763C.
[26] K. Sugioka, A. Kodama-Takahshi, T. Sato, K. Okada, J. Murakami, A.-M. Park, H. Mishima, Y. Shimomura, S. Kusaka, T. Nishida, Plasminogen-dependent collagenolytic properties of *Staphylococcus aureus* in collagen gel cultures of human corneal fibroblasts, Invest. Ophthalmol. Vis. Sci. 59 (2018) 5098, doi:10.1167/iovs.18-24925.
[27] Á. Jacobsen, S.-O. Mikalsen, H. Joensen, J. Eysturskarð, Composition and dynamics of the bacterial communities present in the post-slaughter environment of farmed Atlantic salmon (*Salmo salar* L.) and correlations to gelatin degrading activity, PeerJ 7 (2019) e7040, doi:10.7717/peerj.7040.
[28] R.L. Nation, J. Li, Colistin in the 21st century, Curr. Opin. Infect. Dis. 22 (2009) 535–543, doi:10.1097/QCO.0b013e328332e672.
[29] M. Klinger-Strobel, C. Stein, C. Forstner, O. Makarewicz, M.W. Pletz, Effects of colistin on biofilm matrices of Escherichia coli and Staphylococcus aureus, Int. J. Antimicrob. Agents 49 (2017) 472–479, doi:10.1016/j.ijantimicag.2017.01.005.
[30] Thomas Subramaniam, Jambhrunkar Gustafsson, Prestidge Kidd, Rifampicin-loaded mesoporous silica nanoparticles for the treatment of intracellular infections, Antibiotics 8 (2019) 39, doi:10.3390/antibiotics8020039.
[31] J.A. Barman Balfour, L.R. Wiseman, Moxifloxacin, Drugs 57 (1999) 363–373, doi:10.2165/00003495-199957030-00007.
[32] R. San Juan, A. Garcia-Reyne, P. Caba, F. Chaves, C. Resines, F. Llanos, F. López-Medrano, M. Lizasoain, J.M. Aguado, Safety and efficacy of moxifloxacin monotherapy for treatment of orthopedic implant-related staphylococcal infections, Antimicrob. Agents Chemother. 54 (2010) 5161–5166, doi:10.1128/AAC.00027-10.
[33] L. Malincarne, M. Ghebregzabher, M.V. Moretti, A.M. Egidi, B. Canovari, G. Tavolieri, D. Francisci, G. Cerulli, F. Baldelli, Penetration of moxifloxacin into bone in patients undergoing total knee arthroplasty, J. Antimicrob. Chemother. 57 (2006) 950–954, doi:10.1093/jac/dkl091.
[34] V. Soranoglou, I. Galanopoulos, E.J. Giamarellos-Bourboulis, A. Papalois, E. Giannitsioti, L.A. Poultsides, T. Choreftaki, K. Kanellakopoulou, Efficacy of intramuscular moxifloxacin in the treatment of experimental osteomyelitis caused by methicillin-resistant Staphylococcus aureus, Int. J. Antimicrob. Agents 50 (2017) 186–190, doi:10.1016/j.ijantimicag.2017.01.041.
[35] D.M. Rothstein, Rifamycins, alone and in combination, Cold Spring Harb. Perspect. Med. 6 (2016) a027011, doi:10.1101/cshperspect.a027011.
[36] E. Forsblom, E. Ruotsalainen, A. Järvinen, Improved outcome with early rifampicin combination treatment in methicillin-sensitive Staphylococcus aureus bacteraemia with a deep infection focus - a retrospective cohort study, PLoS One 10 (2015) e0122824, doi:10.1371/journal.pone.0122824.
[37] B. Leijtens, J.B.W. Elbers, P.D. Sturm, B.J. Kullberg, B.W. Schreurs, Clindamycin-rifampin combination therapy for staphylococcal periprosthetic joint infections: a retrospective observational study, BMC Infect. Dis. 17 (2017) 321, doi:10.1186/s12879-017-2429-2.
[38] F. Greimel, C. Scheuerer, A. Gessner, M. Simon, T. Kalteis, J. Grifka, A. Benditz, H.-R. Springorum, J. Schaumburger, Efficacy of antibiotic treatment of implant-associated Staphylococcus aureus infections with moxifloxacin, flucloxacillin, rifampin, and combination therapy: an animal study, DDDT 11 (2017) 1729–1736, doi:10.2147/DDDT.S138888.
[39] Á. Auñón, J. Esteban, A.L. Doadrio, M. Boiza-Sánchez, A. Mediero, D. Eguibar-Blázquez, J. Cordero-Ampuero, A. Conde, M. Arenas, J. de-Damborenea, J.J. Aguilera-Correa, *Staphylococcus aureus* prosthetic joint infection is prevented by a fluorine- and phosphorus-doped nanostructured Ti–6Al–4V alloy loaded with gentamicin and vancomycin, J. Orthop. Res. 38 (2020) 588–597, doi:10.1002/jor.24496.
[40] A.L. Doadrio, A. Conde, M.A. Arenas, J.M. Hernández-López, J.J. de Damborenea, C. Pérez-Jorge, J. Esteban, M. Vallet-Regí, Use of anodized titanium alloy as drug carrier: ibuprofen as model of drug releasing, Int. J. Pharm. 492 (2015) 207–212, doi:10.1016/j.ijpharm.2015.07.046.
[41] J.-J. Aguilera-Correa, A.L. Doadrio, A. Conde, M.-A. Arenas, J.-J. de-Damborenea, M. Vallet-Regí, J. Esteban, Antibiotic release from F-doped nanotubular oxide layer on TI6AL4V alloy to decrease bacterial viability, J. Mater. Sci. Mater. Med. 29 (2018) 118, doi:10.1007/s10856-018-6119-4.
[42] S.S. Aiken, J.J. Cooper, H. Florance, M.T. Robinson, S. Michell, Local release of antibiotics for surgical site infection management using high-purity calcium sulfate: an in vitro elution study, Surg Infect 16 (2015) 54–61, doi:10.1089/sur.2013.162.
[43] L.É. Uhljar, S.Y. Kan, N. Radacsi, V. Koutsos, P. Szabó-Révész, R. Ambrus, In vitro drug release, permeability, and structural test of ciprofloxacin-loaded nanofibers, Pharmaceutics 13 (2021) 556, doi:10.3390/pharmaceutics13040556.
[44] J.A. Ocaña, F.J. Barragán, M. Callejón, Spectrofluorimetric determination of moxifloxacin in tablets, human urine and serum, Analyst 125 (2000) 2322–2325, doi:10.1039/b005991i.
[45] S. Benetton, Visible spectrophotometric and first-derivative UV spectrophotometric determination of rifampicin and isoniazid in pharmaceutical preparations, Talanta 47 (1998) 639–643, doi:10.1016/S0039-9140(98)00111-8.
[46] S. Kasugai, R. Fujisawa, Y. Waki, K. Miyamoto, K. Ohya, Selective drug delivery system to bone: small peptide (Asp)6 conjugation, J. Bone Miner. Res. 15 (2000) 936–943, doi:10.1359/jbmr.2000.15.5.936.
[47] R.D. Plaut, C.P. Mocca, R. Prabhakara, T.J. Merkel, S. Stibitz, Stably luminescent Staphylococcus aureus clinical strains for use in bioluminescent imaging, PLoS One 8 (2013) e59232, doi:10.1371/journal.pone.0059232.
[48] S. Stepanović, D. Vuković, V. Hola, G. Di Bonaventura, S. Djukić, I. Cirković, F. Ruzicka, Quantification of biofilm in microtiter plates: overview of testing conditions and practical recommendations for assessment of biofilm production by staphylococci, APMIS 115 (2007) 891–899, doi:10.1111/j.1600-0463.2007.apm_630.x.
[49] J.M. Mootz, M.A. Benson, C.E. Heim, H.A. Crosby, J.S. Kavanaugh, P.M. Dunman, T. Kielian, V.J. Torres, A.R. Horswill, Rot is a key regulator of *S taphylococcus aureus* biofilm formation: rot regulates *S . aureus* biofilm formation, Mol. Microbiol. 96 (2015) 388–404, doi:10.1111/mmi.12943.
[50] M.P. Weinstein, Methods for dilution antimicrobial susceptibility tests for bacteria that grow aerobically, 2018.
[51] C. Hernandes, J. da S. Coppede, B.W. Bertoni, S. de C. França, A.M.S. Pereira, A rapid and economic method for determination of MBC and MFC, AJPS 04 (2013) 850–852, doi:10.4236/ajps.2013.44104.
[52] E. Grela, J. Kozłowska, A. Grabowiecka, Current methodology of MTT assay in bacteria – a review, Acta Histochem. 120 (2018) 303–311, doi:10.1016/j.acthis.2018.03.007.
[53] I.N. Okoliegbe, K. Hijazi, K. Cooper, C. Ironside, I.M. Gould, Antimicrobial synergy testing: comparing the tobramycin and ceftazidime gradient diffusion methodology used in assessing synergy in cystic fibrosis-derived multidrug-resistant Pseudomonas aeruginosa, Antibiotics 10 (2021) 967, doi:10.3390/antibiotics10080967.
[54] A.L. Leber, Synergism testing: broth microdilution checkerboard and broth macrodilution methods, Clinical Microbiology Procedures Handbook, ASM Press, Washington, DC, USA, 2016 p. 5.16.1-5.16.23, doi:10.1128/9781555818814.ch5.16.
[55] European Committee for Antimicrobial Susceptibility Testing (EUCAST) of the European Society of Clinical Microbiology and Infectious Dieases (ESCMID), EUCAST Definitive Document E.Def 1.2, May 2000: Terminology relating to methods for the determination of susceptibility of bacteria to antimicrobial agents, Clin. Microbiol. Infect. 6 (2000) 503–508, doi:10.1046/j.1469-0691.2000.00149.x.
[56] F.C. Odds, Synergy, antagonism, and what the chequerboard puts between them, J. Antimicrob. Chemother. 52 (2003) 1–1, doi:10.1093/jac/dkg301.
[57] J.J. Aguilera-Correa, M. Gisbert-Garzarán, A. Mediero, R.A. Carias-Cálix, C. Jiménez-Jiménez, J. Esteban, M. Vallet-Regí, Arabic gum plus colistin coated moxifloxacin-loaded nanoparticles for the treatment of bone infection caused by Escherichia coli, Acta Biomater. 137 (2022) 218–237, doi:10.1016/j.actbio.2021.10.014.
[58] S. DeLeon, A. Clinton, H. Fowler, J. Everett, A.R. Horswill, K.P. Rumbaugh, Synergistic interactions of Pseudomonas aeruginosa and Staphylococcus aureus in an in vitro wound model, Infect. Immun. 82 (2014) 4718–4728, doi:10.1128/IAI.02198-14.
[59] Z. Gounani, M.A. Asadollahi, Jannik.N. Pedersen, J. Lyngsø, J. Skov Pedersen, A. Arpanaei, R.L. Meyer, Mesoporous silica nanoparticles carrying multiple antibiotics provide enhanced synergistic effect and improved biocompatibility, Colloids Surf. B 175 (2019) 498–508, doi:10.1016/j.colsurfb.2018.12.035.
[60] E. Peeters, H.J. Nelis, T. Coenye, In vitro activity of ceftazidime, ciprofloxacin, meropenem, minocycline, tobramycin and trimethoprim/sulfamethoxazole against planktonic and sessile Burkholderia cepacia complex bacteria, J. Antimicrob. Chemother. 64 (2009) 801–809, doi:10.1093/jac/dkp253.
[61] J. Esteban, E. Gomez-Barrena, J. Cordero, N.Z. Martín-de-Hijas, T.J. Kinnari, R. Fernandez-Roblas, Evaluation of quantitative analysis of cultures from son-

icated retrieved orthopedic implants in diagnosis of orthopedic infection, J. Clin. Microbiol. 46 (2008) 488–492, doi:10.1128/JCM.01762-07.
[62] B. Herigstad, M. Hamilton, J. Heersink, How to optimize the drop plate method for enumerating bacteria, J. Microbiol. Methods 44 (2001) 121–129, doi:10.1016/s0167-7012(00)00241-4.
[63] G.J. Oostingh, E. Casals, P. Italiani, R. Colognato, R. Stritzinger, J. Ponti, T. Pfaller, Y. Kohl, D. Ooms, F. Favilli, H. Leppens, D. Lucchesi, F. Rossi, I. Nelissen, H. Thielecke, V.F. Puntes, A. Duschl, D. Boraschi, Problems and challenges in the development and validation of human cell-based assays to determine nanoparticle-induced immunomodulatory effects, Part. Fibre Toxicol. 8 (8) (2011), doi:10.1186/1743-8977-8-8.
[64] S.S. Hakki, B.S. Bozkurt, E.E. Hakki, Boron regulates mineralized tissue-associated proteins in osteoblasts (MC3T3-E1), J. Trace Elem. Med. Biol. 24 (2010) 243–250, doi:10.1016/j.jtemb.2010.03.003.
[65] X. Yuan, H. Cao, J. Wang, K. Tang, B. Li, Y. Zhao, M. Cheng, H. Qin, X. Liu, X. Zhang, Immunomodulatory effects of calcium and strontium co-doped titanium oxides on osteogenesis, Front. Immunol. 8 (2017) 1196, doi:10.3389/fimmu.2017.01196.
[66] A.Y. Ng, C. Tu, S. Shen, D. Xu, M.J. Oursler, J. Qu, S. Yang, Comparative characterization of osteoclasts derived from murine bone marrow macrophages and RAW 264.7 cells using quantitative proteomics: proteomic comparison of osteoclast models, JBMR Plus 2 (2018) 328–340, doi:10.1002/jbm4.10058.
[67] T.L. Riss, R.A. Moravec, A.L. Niles, S. Duellman, H.A. Benink, T.J. Worzella, L. Minor, Cell viability assays, in: S. Markossian, A. Grossman, K. Brimacombe, M. Arkin, D. Auld, C.P. Austin, J. Baell, T.D.Y. Chung, N.P. Coussens, J.L. Dahlin, V. Devanarayan, T.L. Foley, M. Glicksman, M.D. Hall, J.V. Haas, S.R.J. Hoare, J. Inglese, P.W. Iversen, S.C. Kales, M. Lal-Nag, Z. Li, J. McGee, O. McManus, T. Riss, P. Saradjian, G.S. Sittampalam, M. Tarselli, O.J. Trask, Y. Wang, J.R. Weidner, M.J. Wildey, K. Wilson, M. Xia, X. Xu (Eds.), Assay Guidance Manual, Eli Lilly & Company and the National Center for Advancing Translational Sciences, Bethesda (MD), 2004 http://www.ncbi.nlm.nih.gov/books/NBK144065/ (accessed October 2, 2021).
[68] F. Faul, E. Erdfelder, A.-G. Lang, A. Buchner, G*Power 3: a flexible statistical power analysis program for the social, behavioral, and biomedical sciences, Behav. Res. Methods 39 (2007) 175–191, doi:10.3758/bf03193146.
[69] J.-J. Aguilera-Correa, Á. Auñón, M. Boiza-Sánchez, I. Mahillo-Fernández, A. Mediero, D. Eguibar-Blázquez, A. Conde, M.-Á. Arenas, J.-J. de-Damborenea, J. Cordero-Ampuero, J. Esteban, Urine aluminum concentration as a possible implant biomarker of *Pseudomonas aeruginosa* infection using a fluorine- and phosphorus-doped Ti-6Al-4V alloy with osseointegration capacity, ACS Omega 4 (2019) 11815–11823, doi:10.1021/acsomega.9b00898.
[70] J.L. Paris, M.V. Cabañas, M. Manzano, M. Vallet-Regí, Polymer-grafted mesoporous silica nanoparticles as ultrasound-responsive drug carriers, ACS Nano 9 (2015) 11023–11033, doi:10.1021/acsnano.5b04378.
[71] F. Balas, M. Manzano, M. Colilla, M. Vallet-Regí, L-Trp adsorption into silica mesoporous materials to promote bone formation, Acta Biomater. 4 (2008) 514–522, doi:10.1016/j.actbio.2007.11.009.
[72] K. Tam, V.J. Torres, Staphylococcus aureus secreted toxins and extracellular enzymes, Microbiol. Spectr. 7 (2019), doi:10.1128/microbiolspec.GPP3-0039-2018.
[73] J. Potempa, J. Travis, in: Aureolysin, in: Handbook of Proteolytic Enzymes, Elsevier, 2004, pp. 389–393, doi:10.1016/B978-0-12-079611-3.50104-X.
[74] A.J. Loughran, D.N. Atwood, A.C. Anthony, N.S. Harik, H.J. Spencer, K.E. Beenken, M.S. Smeltzer, Impact of individual extracellular proteases on *Staphylococcus aureus* biofilm formation in diverse clinical isolates and their isogenic *sarA* mutants, MicrobiologyOpen 3 (2014) 897–909, doi:10.1002/mbo3.214.
[75] H. Devlin, S. Fulaz, D.W. Hiebner, J.P. O'Gara, E. Casey, Enzyme-functionalized mesoporous silica nanoparticles to target Staphylococcus aureus and disperse biofilms, IJN 16 (2021) 1929–1942, doi:10.2147/IJN.S293190.
[76] C. Mateo, J.M. Palomo, G. Fernandez-Lorente, J.M. Guisan, R. Fernandez-Lafuente, Improvement of enzyme activity, stability and selectivity via immobilization techniques, Enzyme Microb. Technol. 40 (2007) 1451–1463, doi:10.1016/j.enzmictec.2007.01.018.
[77] I.I. Momodu, V. Savaliya, Osteomyelitis, StatPearls, StatPearls Publishing, Treasure Island (FL), 2022 http://www.ncbi.nlm.nih.gov/books/NBK532250/ (accessed February 25, 2022).
[78] D. Minardi, M.P. Montanari, E. Tili, I. Cochetti, M. Mingoia, P.E. Varaldo, G. Muzzonigro, Effects of fluoroquinolones on bacterial adhesion and on preformed biofilm of strains isolated from urinary double J stents, J. Chemother. 20 (2008) 195–201, doi:10.1179/joc.2008.20.2.195.
[79] M.J. González, L. Robino, V. Iribarnegaray, P. Zunino, P. Scavone, Effect of different antibiotics on biofilm produced by uropathogenic Escherichia coli isolated from children with urinary tract infection, Pathog. Dis. (2017) 75, doi:10.1093/femspd/ftx053.
[80] A. Aguilar-Colomer, J.C. Doadrio, C. Pérez-Jorge, M. Manzano, M. Vallet-Regí, J. Esteban, Antibacterial effect of antibiotic-loaded SBA-15 on biofilm formation by Staphylococcus aureus and Staphylococcus epidermidis, J. Antibiot. 70 (2017) 259–263, doi:10.1038/ja.2016.154.
[81] C.L. Brinkman, S.M. Schmidt-Malan, J.N. Mandrekar, R. Patel, Rifampin-based combination therapy is active in foreign-body osteomyelitis after prior rifampin monotherapy, Antimicrob. Agents Chemother. 61 (2017) e01822-16, doi:10.1128/AAC.01822-16.
[82] W. Zimmerli, P. Sendi, Role of rifampin against staphylococcal biofilm infections in vitro, in animal models, and in orthopedic-device-related infections, Antimicrob. Agents Chemother. 63 (2019) e01746-18, doi:10.1128/AAC.01746-18.
[83] I. Marriott, Apoptosis-associated uncoupling of bone formation and resorption in osteomyelitis, Front. Cell Infect. Microbiol. 3 (2013) 101, doi:10.3389/fcimb.2013.00101.
[84] Y.-T. Liao, C.-H. Lee, S.-T. Chen, J.-Y. Lai, K.C.-W. Wu, Gelatin-functionalized mesoporous silica nanoparticles with sustained release properties for intracameral pharmacotherapy of glaucoma, J. Mater. Chem. B. 5 (2017) 7008–7013, doi:10.1039/C7TB01217A.
[85] X. Zhou, W. Weng, B. Chen, W. Feng, W. Wang, W. Nie, L. Chen, X. Mo, J. Su, C. He, Mesoporous silica nanoparticles/gelatin porous composite scaffolds with localized and sustained release of vancomycin for treatment of infected bone defects, J. Mater. Chem. B. 6 (2018) 740–752, doi:10.1039/C7TB01246B.
[86] J.-H. Xu, F.-P. Gao, L.-L. Li, H.L. Ma, Y.-S. Fan, W. Liu, S.-S. Guo, X.-Z. Zhao, H. Wang, Gelatin–mesoporous silica nanoparticles as matrix metalloproteinases-degradable drug delivery systems in vivo, Microporous Mesoporous Mater. 182 (2013) 165–172, doi:10.1016/j.micromeso.2013.08.050.
[87] Z. Zou, D. He, X. He, K. Wang, X. Yang, Z. Qing, Q. Zhou, Natural gelatin capped mesoporous silica nanoparticles for intracellular acid-triggered drug delivery, Langmuir 29 (2013) 12804–12810, doi:10.1021/la4022646.
[88] B. Zhang, Z. Ding, J. Dong, F. Lin, Z. Xue, J. Xu, Macrophage-mediated degradable gelatin-coated mesoporous silica nanoparticles carrying pirfenidone for the treatment of rat spinal cord injury, Nanomed. Nanotechnol. Biol. Med. 37 (2021) 102420, doi:10.1016/j.nano.2021.102420.
[89] C. Fu, H. Bai, Q. Hu, T. Gao, Y. Bai, Enhanced proliferation and osteogenic differentiation of MC3T3-E1 pre-osteoblasts on graphene oxide-impregnated PLGA–gelatin nanocomposite fibrous membranes, RSC Adv. 7 (2017) 8886–8897, doi:10.1039/C6RA26020A.
[90] J. Liu, B. Zhang, S. Song, M. Ma, S. Si, Y. Wang, B. Xu, K. Feng, J. Wu, Y. Guo, Bovine collagen peptides compounds promote the proliferation and differentiation of MC3T3-E1 pre-osteoblasts, PLoS One 9 (2014) e99920, doi:10.1371/journal.pone.0099920.
[91] R. Rohanizadeh, M.V. Swain, R.S. Mason, Gelatin sponges (Gelfoam) as a scaffold for osteoblasts, J. Mater. Sci. Mater. Med. 19 (2008) 1173–1182, doi:10.1007/s10856-007-3154-y.
[92] A.Y. Kim, Y. Kim, S.H. Lee, Y. Yoon, W.-H. Kim, O.-K. Kweon, Effect of gelatin on osteogenic cell sheet formation using canine adipose-derived mesenchymal stem cells, Cell Transplant. 26 (2017) 115–123, doi:10.3727/096368916X693338.
[93] M.E. Abdelgawad, K. Søe, T.L. Andersen, D.M.H. Merrild, P. Christiansen, P. Kjærsgaard-Andersen, J.-M. Delaisse, Does collagen trigger the recruitment of osteoblasts into vacated bone resorption lacunae during bone remodeling? Bone 67 (2014) 181–188, doi:10.1016/j.bone.2014.07.012.
[94] B. Kruppke, S. Ray, V. Alt, M. Rohnke, C. Kern, M. Kampschulte, C. Heinemann, M. Budak, J. Adam, N. Döhner, L. Franz-Forsthoffer, T. El Khassawna, C. Heiss, T. Hanke, U. Thormann, Gelatin-modified calcium/strontium hydrogen phosphates stimulate bone regeneration in osteoblast/osteoclast co-culture and in osteoporotic rat femur defects-in vitro to in vivo translation, Molecules 25 (2020) E5103, doi:10.3390/molecules25215103.
[95] S. Lee, J. Kim, K. Ravichandran, H.-W. Gil, H. Song, S. Hong, P-Glycoprotein induction ameliorates colistin induced nephrotoxicity in cultured human proximal tubular cells, PLoS One 10 (2015) e0136075, doi:10.1371/journal.pone.0136075.
[96] B. Sobolewska, J. Hofmann, M.S. Spitzer, K.U. Bartz-Schmidt, P. Szurman, E. Yoeruek, Antiproliferative and cytotoxic properties of moxifloxacin on rat retinal ganglion cells, Curr. Eye Res. 38 (2013) 662–669, doi:10.3109/02713683.2012.746991.
[97] L. Bassi, L.D. Berardino, V. Arioli, L.G. Silvestri, E.L.C. Lignière, Conditions for immunosuppression by rifampicin, J. Infect. Dis. 128 (1973) 736–744.
[98] S.G. Moore, K.L. Dawson, Red and yellow marrow in the femur: age-related changes in appearance at MR imaging, Radiology 175 (1990) 219–223, doi:10.1148/radiology.175.1.2315484.
[99] M. Sritharan, Studies on the tissue distribution of liposome-associated clofazimine, an antileprosy drug, Methods Find Exp. Clin. Pharmacol. 15 (1993) 107–111.
[100] S. Lee, M.-S. Kim, D. Lee, T.K. Kwon, D. Khang, H.-S. Yun, S.-H. Kim, The comparative immunotoxicity of mesoporous silica nanoparticles and colloidal silica nanoparticles in mice, Int J Nanomedicine 8 (2013) 147–158, doi:10.2147/IJN.S39534.
[101] K. Brandl, V. Kumar, L. Eckmann, Gut-liver axis at the frontier of host-microbial interactions, Am. J. Physiol.-Gastrointestinal Liver Physiol. 312 (2017) G413–G419, doi:10.1152/ajpgi.00361.2016.
[102] W.H. Taliaferro, L.G. Taliaferro, The role of the spleen in hemolysin production in rabbits receiving multiple antigen injections, J. Infect. Dis. 89 (1951) 143–168, doi:10.1093/infdis/89.2.143.
[103] F. Vandenesch, G. Lina, T. Henry, Staphylococcus aureus hemolysins, bi-component leukocidins, and cytolytic peptides: a redundant arsenal of membrane-damaging virulence factors? Front. Cell. Inf. Microbio. 2 (2012), doi:10.3389/fcimb.2012.00012.
[104] M. Honda, B.G.J. Surewaard, M. Watanabe, C.C. Hedrick, W.-Y. Lee, K. Brown, K.D. McCoy, P. Kubes, Perivascular localization of macrophages in the intestinal mucosa is regulated by Nr4a1 and the microbiome, Nat. Commun. 11 (2020) 1329, doi:10.1038/s41467-020-15068-4.